

# STATISTICAL MECHANICS OF GENERALIZATION IN GRAPH CONVOLUTION NETWORKS

CHENG SHI<sup>1</sup>, LIMING PAN<sup>2</sup>, HONG HU<sup>3</sup>, IVAN DOKMANIĆ<sup>1,4,\*</sup>

**ABSTRACT.** Graph neural networks (GNN) have become the default machine learning model for relational datasets, including protein interaction networks, biological neural networks, and scientific collaboration graphs. We use tools from statistical physics and random matrix theory to precisely characterize generalization in simple graph convolution networks on the contextual stochastic block model. The derived curves are phenomenologically rich: they explain the distinction between learning on homophilic and heterophilic graphs and they predict double descent whose existence in GNNs has been questioned by recent work. Our results are the first to accurately explain the behavior not only of a stylized graph learning model but also of complex GNNs on messy real-world datasets. To wit, we use our analytic insights about homophily and heterophily to improve performance of state-of-the-art graph neural networks on several heterophilic benchmarks by a simple addition of negative self-loop filters.

## 1. INTRODUCTION

In machine learning we often assume that data are independent random variables with some unknown probability distribution. A more powerful paradigm is to leverage relational information: In a dataset of proteins we may know which ones interact; in a literature corpus we may know which articles reference each other; in a dataset of statisticians we may know which ones collaborate. A natural mathematical model is then a combinatorial graph and the *de facto* machine learning model a graph neural network [8, 15, 19, 23].

In this paper we study generalization of graph neural networks in semi-supervised (transductive) node classification: given a graph  $G = (V, E)$ , node features  $\mathbf{x} : V \rightarrow \mathbb{R}^F$ , and labels  $y : V_{\text{train}} \rightarrow \{-1, 1\}$  for a “training” subset of nodes  $V_{\text{train}} \subset V$ , we want to learn a rule which assigns labels to nodes in  $V_{\text{test}} = V \setminus V_{\text{train}}$ . We are interested in the behavior of the generalization error as a function of the domain-specific parameters: amount of noise in the graph, amount of noise in the node features, proportion of observed labels  $|V_{\text{train}}|/|V|$ , and the “type” of interactions encoded in the graph.

Most theoretical work on GNNs addresses their expressivity [17, 44]. A key result is that the common message-passing formulation is limited by the power of the Weisfeiler–Lehman graph isomorphism test [55]. This is of great relevance for computational chemistry where one must discriminate between the different molecular structures [18], but it does not explain how the interaction between the graph structure and the node features leads to strong generalization. Indeed, simple architectures like graph convolution networks (GCN) are far from being universal approximators but they often achieve excellent performance on real problems with real data.

Existing studies of generalization in GNNs leverage complexity measures such as the Vapnik–Chervonenkis dimension [45] or the Rademacher complexity [16]. While the resulting bounds predict coarse qualitative behavior, a precise characterization of emergent phenomena remains elusive. Even sophisticated techniques like PAC-Bayes perform only marginally better [25]. It

<sup>1</sup> DEPARTEMENT MATHÉMATIK UND INFORMATIK, UNIVERSITÄT BASEL

<sup>2</sup> SCHOOL OF COMPUTER AND ELECTRONIC INFORMATION, NANJING NORMAL UNIVERSITY

<sup>3</sup> WHARTON DEPARTMENT OF STATISTICS AND DATA SCIENCE, UNIVERSITY OF PENNSYLVANIA

<sup>4</sup> DEPARTMENT OF ELECTRICAL AND COMPUTER ENGINEERING, UNIVERSITY OF ILLINOIS AT URBANA-CHAMPAIGN  
E-mail address: [ivan.dokmanic@unibas.ch](mailto:ivan.dokmanic@unibas.ch).

Date: December, 2022.

*Key words and phrases.* Graph neural network, graph convolution network, transductive learning, Replica method, random matrix theory, generalization, double descent, stochastic block model, geometric deep learning.

is striking that only in rare cases these bounds explicitly incorporate the interaction between the graph and the features [14]. Here we show that understanding this interaction is crucial to understand learning on graphs.

To see this intuitively, recall that a standard practice in the design of GNNs is to build (generalized) filters from the adjacency matrix or the graph Laplacian and then use these filters to process data. But if the underlying graph is an Erdős–Rényi random graph, the induced filters will be of little use in learning. We should thus understand how much useful information the graph provides about the labels (and vice-versa), and in what way is that information complementary to that contained in the features.

Instead of complexity-based generalization bounds, we study performance of simple but representative graph convolution networks on a concrete random graph ensemble: the contextual stochastic block model (CSBM) [10]. This allows us to derive precise expressions for the learning curves which exhibit a rich phenomenology. Our expressions for test risk explain the important qualitative differences between learning on homophilic and heterophilic graphs. In Section 3.3 we show why self-loops greatly improve performance of GNNs on homophilic [30] but not heterophilic [7, 40] graphs—an observation that has been empirically established in a number of papers—but also that *negative* self-loops similarly benefit learning on heterophilic graphs. We also predict a double descent phenomenon for transductive graph learning: there exists a (perhaps counterintuitive) regime where more training data *hurts* generalization. This is remarkable because recent work points out that double descent has not yet been observed in graph learning, possibly due to implicit regularization [36].

We then turn to large state-of-the-art models trained on real datasets and show that our findings apply there as well. We can in fact leverage our analytic observations about positive and negative self-loops to design better GCNs. We modify a state-of-the-art graph neural network FSGNN [29] in a very simple way, by adding negative self-loops, and obtain new state-of-the-art results on several heterophilic benchmarks.

**1.1. Precise analysis of simple models.** The complexity-based risk bounds are typically vacuous for modern machine learning models; this is certainly the case for graph neural networks [14, 16, 25]. There is a tradeoff between the generality of such bounds and the precision of model-based approaches which assume a concrete data-generating distribution.

Our results belong to the latter group. They resemble results derived over the last decade for regularized least-squares [5, 38, 49], random-feature regression [4, 21, 31], and noisy Gaussian mixture and spiked covariance models [2, 13, 33], using a variety of analytical techniques from statistical physics, high-dimensional probability, and random matrix theory.

Even though these papers study simple models, a number of key results only appeared in the last couple of years, motivated by the proliferation of over-parameterized models and advances in analytical techniques. We extend these results by allowing the information to propagate on a graph and show that this gives rise to a rich new phenomenology. At the level of analysis it results in products of random adjacency matrices and random feature matrices. In order to obtain precise results we similarly study simple, shallow graph networks, but we also show that the salient predictions hold true in state-of-the-art networks and real datasets.

**1.2. (Semi)supervised, unsupervised, Bayesian.** One interpretation of our analysis is that it quantifies the value of (a small amount of) labeled data in problems that are traditionally approached by unsupervised learning. These approaches are subject to fundamental information-theoretic detection limits [9, 13, 34] which have drawn considerable attention over the last decade. The most challenging and most realistic high-dimensional setting is when the signal strength is comparable to that of the noise for both the graph and the features that live on the graph [9, 10]. We show that a small fraction of labeled data breaks these detection barriers even with a simple model like a shallow graph convolution network.

To derive our results we leverage analytical techniques from statistical physics. We use the replica method to isolate the influence of the random adjacency matrix and to demonstrate that the binary adjacency matrix may be replaced by a spiked Gaussian matrix without changing the asymptotic risk, which is a form of universality. This in turn allows us to derive expressions for

generalization risk and accuracy, in some cases in closed form and in general as a solution to a low-dimensional saddle point problem.

## 2. PROBLEM SETUP AND BACKGROUND

**2.1. Notation.** We denote matrices by uppercase ( $\mathbf{Q}$ ) and vectors by lowercase ( $\mathbf{m}$ ) boldface letters. We use subscripts to index their entries ( $\mathbf{Q}_{ab}, \mathbf{m}_a$ ) and superscripts to index vectors in a sequence ( $\mathbf{x}^i$ ). The symbol  $\mathbf{1}_n$  denotes the vector of all ones;  $\mathbf{I}_n$  denotes the  $n \times n$  identity matrix. We write  $|S|$  for the cardinality of a set  $S$ . Throughout the paper we write  $\mathbf{A}$  for the  $N \times N$  adjacency matrix of the graph  $G = (V, E)$  so that  $\mathbf{A}_{uv} = 1$  if there is an edge between  $u, v \in V$ , and  $\mathbf{A}_{uv} = 0$  otherwise. We collect the  $F$ -dimensional features for all  $N$  nodes in the rows of the  $N \times F$  matrix  $\mathbf{X}$ .

**2.2. Semi-supervised node classification with a simple GCN.** Graph convolution networks are composed of graph convolution filters and nonlinear activation functions. Removing the activations results in a so-called simple GCN [54] or a spectral GNN [20, 52],

$$(1) \quad h(\mathbf{w}; \mathbf{A}, \mathbf{X}) = \mathbf{P}(\mathbf{A})\mathbf{X}\mathbf{w} \quad \text{where} \quad \mathbf{P}(\mathbf{A}) = \sum_{k=0}^K c_k \mathbf{A}^k,$$

where  $\mathbf{w} \in \mathbb{R}^F$  are trainable parameters and  $K$  is the filter support size in terms of hops on the graph. We treat the neighborhood weights at different hops  $c_k$  as hyperparameters. We let  $\mathbf{A}^0 \stackrel{\text{def}}{=} \mathbf{I}_N$  so that the model (1) reduces to ordinary linear regression when  $K = 0$ .

**2.3. GCNs without activations.** Removing activations may seem like a gross simplification. In standard feed-forward networks it indeed results in a linear end-to-end mapping, but recent studies surprisingly show that graph convolution networks without activations (such as SGC [54]) or with activations only in the output (such as FSGNN [29] and GPRGNN [7]) achieve state-of-the-art performance on common benchmarks. Indeed, we will derive risk expressions for the above graph convolution network in two shallow cases:  $\mathbf{P}(\mathbf{A}) = \mathbf{A}$  and  $\mathbf{P}(\mathbf{A}) = \mathbf{A} + c\mathbf{I}$  and state a universality conjecture for general polynomial filters. But we will also show that the phenomena observed on these models also exist in graph networks with non-linear activations and the principles that improve generalization on simple models also benefit the complex state-of-the-art models.

We remark that although graph networks without activations are sometimes called “linear” in analogy with feed-forward networks without activations, that terminology is misleading. In graph learning both  $\mathbf{A}$  and  $\mathbf{X}$  are bona fide parts of the input and a function which depends on their multiplication is a nonlinear function. What is more, in many applications  $\mathbf{A}$  is constructed deterministically from a dataset  $\mathbf{X}$ , for example as a neighborhood graph, resulting in even stronger nonlinearity.

**2.4. Training and generalization.** We are interested in the large graph limit  $N \rightarrow \infty$  where the training ratio  $|V_{\text{train}}|/N \rightarrow \tau$ . We fit the model parameters  $\mathbf{w}$  by ridge regression,

$$(2) \quad \mathbf{w}^* := \arg \min_{\mathbf{w}} L_{\mathbf{A}, \mathbf{X}}(\mathbf{w}), \quad \text{where} \quad L_{\mathbf{A}, \mathbf{X}}(\mathbf{w}) = \frac{1}{|V_{\text{train}}|} \sum_{i \in V_{\text{train}}} (\mathbf{y}_i - (\mathbf{h}_i(\mathbf{w})))^2 + \frac{r}{N} \|\mathbf{w}\|_2^2.$$

We are interested in the training and test risk in the limit of large graphs,

$$(3) \quad \begin{aligned} R_{\text{train}} &:= \lim_{N \rightarrow \infty} \mathbb{E} \left[ \frac{1}{|V_{\text{train}}|} \sum_{i \in V_{\text{train}}} (\mathbf{y}_i - (\mathbf{h}_i(\mathbf{w}^*)))^2 \right], \\ R_{\text{test}} &:= \lim_{N \rightarrow \infty} \mathbb{E} \left[ \frac{1}{|V_{\text{test}}|} \sum_{i \in V_{\text{test}}} (\mathbf{y}_i - (\mathbf{h}_i(\mathbf{w}^*)))^2 \right], \end{aligned}$$

as well as in the expected accuracy,

$$(4) \quad \text{ACC} := \lim_{N \rightarrow \infty} \mathbb{E} \left[ \frac{1}{|V_{\text{test}}|} \sum_{i \in V_{\text{test}}} \mathbb{1}_{\mathbf{y}_i = \text{sign}(\mathbf{h}_i(\mathbf{w}^*))} \right].$$

The expectations in the above expressions are over the random graph adjacency matrix  $\mathbf{A}$ , random features  $\mathbf{X}$ , and the uniformly random test–train partition  $V = V_{\text{train}} \cup V_{\text{test}}$ . Our analysis in fact shows that the quantities in the arguments of expectations all concentrate around the expectation as  $N \rightarrow \infty$ . (In the language of statistical physics, they are *self-averaging*.)

We will sometimes write  $R_{\text{train}}(\mathcal{A})$ ,  $R_{\text{test}}(\mathcal{A})$ ,  $\text{ACC}(\mathcal{A})$  to emphasize that the matrix  $\mathbf{A}$  in (1) follows a distribution  $\mathcal{A}$ ,  $\mathbf{A} \sim \mathcal{A}$ .

**2.5. Contextual Stochastic Block Model.** The contextual stochastic block model (CSBM) adds node features to the stochastic block model (SBM)—an established random graph model with community structure [10]. In the SBM (or, more precisely, the 2-SBM), the nodes are split into two communities. Links between pairs of nodes are established independently, with different probabilities for links between nodes in the same and in the different communities. The resulting adjacency matrix  $\mathbf{A}^{\text{bs}}$  has the lower triangular part distributed as

$$(5) \quad \mathbb{P}(\mathbf{A}_{ij}^{\text{bs}} = 1) = \begin{cases} c_{\text{in}}/N & \text{if } i \leq j \text{ and } \mathbf{y}_i = \mathbf{y}_j \\ c_{\text{out}}/N & \text{if } i \leq j \text{ and } \mathbf{y}_i \neq \mathbf{y}_j. \end{cases}$$

Adjusting  $c_{\text{in}}$  and  $c_{\text{out}}$  allows us to obtain homophilic and heterophilic graphs with different average node degrees (see Section 3.3). We adopt a convenient parameterization

$$c_{\text{in}} = d + \sqrt{d}\lambda, \quad c_{\text{out}} = d - \sqrt{d}\lambda,$$

where the sign of  $\lambda$  determines whether the graph is homophilic or heterophilic, and the magnitude  $|\lambda|$  can be regarded as the signal noise ratio (SNR) of the graph.

We will also study a non-symmetric (directed) SBM [28, 53] with adjacency matrix distributed as

$$(6) \quad \mathbb{P}(\mathbf{A}_{ij}^{\text{bn}} = 1) = \begin{cases} c_{\text{in}}/N & \text{if } \mathbf{y}_i = \mathbf{y}_j \\ c_{\text{out}}/N & \text{if } \mathbf{y}_i \neq \mathbf{y}_j. \end{cases}$$

Many real networks have directed links, including chemical connections between neurons, the electric grid, follower–follower relation in social media, and Bayesian networks. In our case the directed SBM will facilitate analysis with self-loops while still exhibiting the same qualitative behavior and phenomenology.

The CSBM adds node features to the SBM, following the spiked covariance model,

$$(7) \quad \mathbf{x}^i = \sqrt{\frac{\mu}{N}} \mathbf{y}_i \mathbf{u} + \boldsymbol{\xi}^i,$$

where  $\mathbf{u} \sim \mathcal{N}(0, \mathbf{I}_F/F)$  is the  $F$ -dimensional hidden feature,  $\boldsymbol{\xi}^i \sim \mathcal{N}(0, \mathbf{I}_F/F)$  are i.i.d. Gaussian noise vectors and the parameter  $\mu$  controls the SNR of the features. We scale  $N$  and  $F$  so that  $\frac{N}{F} \rightarrow \gamma$ , with  $\gamma$  being the inverse sampling ratio, and ascribe feature vectors to the rows of the data matrix  $\mathbf{X}$ ,

$$(8) \quad \mathbf{X} = [\mathbf{x}^1, \dots, \mathbf{x}^N]^\top = \sqrt{\frac{\mu}{N}} \mathbf{y} \mathbf{u}^\top + \boldsymbol{\Xi}.$$

Throughout this paper we assume that the two communities are balanced, each with  $\frac{N}{2}$  nodes (assuming even  $N$ ). Without loss of generality we may assume that  $\mathbf{y}_i = 1$  for  $i = 1, 2, \dots, N/2$ , and  $\mathbf{y}_i = -1$  for  $i > N/2$ .

As we show in what follows, the CSBM yields a comparatively tractable statistical model to characterize generalization in graph neural networks. We intuitively expect that with a proper scaling of the model parameters, when  $N \rightarrow \infty$ , the risks will concentrate around a value that

depends on five parameters:

$\lambda$	Graph SNR,
$\mu$	Node features SNR,
$\gamma$	Inverse sampling ratio,
$\tau$	Training ratio,
$r$	Ridge regularization parameter.

We again emphasize that we study the challenging weak-signal regime where  $\lambda$ ,  $\mu$  and  $\gamma$  do not scale with  $N$ . This stands in contrast to recent machine learning work on the CSBM [1, 26] which study the low-noise regime where  $\mu$  or  $\lambda^2$  scale with  $N$ , or even the noiseless signal where the classes become linearly separable after applying a graph filter or a GCN. We argue that the weak-signal regime is closer to real graph learning problems which are neither too easy (as in linearly separable) nor too hard (as with a vanishing signal). The fact that we discover phenomena which also occur in state-of-the-art networks and real datasets supports this claim.

### 3. PHENOMENOLOGY OF GENERALIZATION IN GCNS

The main benefit of precise understanding of stylized models like the CSBM is that it points to important phenomena. We focus on two: i) the qualitative distinction between learning on homophilic and heterophilic graphs and ii) the “double descent” shape of the test risk curves which was not previously reported for graph neural networks.

**3.1. Double descent in one layer GCN on CSBM.** A line of research starting with [3] shows that in modern machine learning models with many parameters, generalization error behaves in a more complicated way than suggested by the traditional U-shaped bias–variance tradeoff. Up to the interpolation point where the model can exactly fit the training data things behave as usual, with the test risk first decreasing together with the bias and then increasing together with the variance due to overfitting. But pushing the model complexity beyond the interpolation point may make the test risk decrease again. A different interpretation is obtained by reading the test risk curve in reverse with appropriate parameter scaling: there exists a regime in which increasing the amount of training data leads to *worse* performance.<sup>1</sup>

This behavior has been theoretically analyzed for many synthetic models but also observed in complex deep neural networks [35]. However, as reported by Oono and Suzuki [36], there are scarcely any reports of double descent in graph neural networks. Oono and Suzuki speculate that this may be due to implicit regularization in relation to oversmoothing. As summarized in Figures 1 and 2, our results show that double descent in graph convolution networks *does* exist.

In transductive learning the double descent can be observed by varying either the (inverse) sampling ratio ( $\gamma = N/F$ ) or the training ratio ( $\tau = |V_{\text{train}}|/|V|$ ). The latter is different from the fully-supervised regime in that we always have access to all the data  $\mathbf{A}$  and  $\mathbf{X}$  but only a subset of labels, and that the amount of training data cannot exceed the number of nodes. The different types of risk curves discussed in the literature can also be observed in our results under different SNRs [4].

The closed-form expression (15) for unregularized regression ( $r = 0$ ) shows that the test error diverges as  $\gamma\tau$  approaches 1. When this happens, the matrix system matrix  $\mathbf{I}_{\text{train}}\mathbf{P}(\mathbf{A})\mathbf{X}$  is square and near-singular for large  $N$ , which leads to the explosion of the test risk (Figure 1A). At the other extreme, for strongly regularized training (large  $r$ ) the double descent disappears (Figure 1C). It has been shown that double descent ceases to exist at optimal regularization. The absolute risk values in Figure 1B and 1C show the same behavior.

<sup>1</sup>Since this is a *double* descent, there are two regions in which more data worsens performance; the surprising one is the first one where there is little data to begin with.

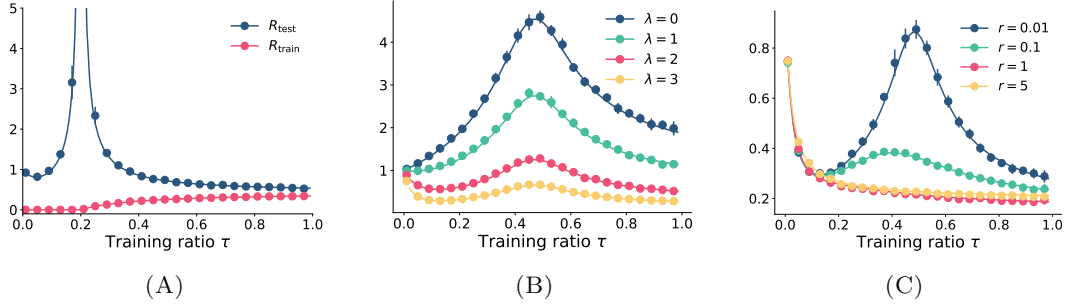


FIGURE 1. Theoretical results computed by the replica method (solid line) vs. experimental results (round dots) on the CSBM, with  $\mathbf{P}(\mathbf{A}) = \mathbf{A}$ , for varying training ratios  $\tau$ . (A): training and test risks with  $\lambda = \mu = 1$ ,  $\gamma = 5$  and  $r = 0$ . (For  $\tau < 0.2$ , we use the pseudoinverse in Equation 9 in numerics and  $r = 10^{-5}$  for the theoretical curves). (B) and (C): test risk with  $r = 0.02$ ,  $\gamma = 2$ ,  $\mu = 1$  in 1B and  $\lambda = 3$ ,  $\mu = 1$ ,  $\gamma = 2$  in 1C. In all plots we set  $N = 5000$  and  $d = 30$ . Each experimental data point is averaged over 10 independent trials and the standard deviation is indicated by vertical lines.

Figure 1B shows that when the graph is very noisy ( $\lambda$  is small) the test risk immediately starts to increase as the training ratio increases from 0. When  $\lambda$  is large, meaning that the graph is discriminative, we have two descents. Similar behavior can be observed when varying the feature SNR  $\mu$  instead of  $\lambda$ . Double descent also appears in test accuracy (Figure 2). In general, the more labels we have, the closer is the mean of the test output to  $\mathbf{y}_i$ . The qualitative differences in the double descent curves arise because the variance of  $\mathbf{h}_i(\mathbf{w}^*)$  behaves differently under different sampling ratios and regularization strengths (cf. Appendix A.1).

For example, when  $r \rightarrow 0$  and  $\tau \rightarrow \frac{1}{\gamma}$ , the variance of  $\mathbf{h}_i(\mathbf{w}^*)$  diverges and the accuracy approaches 50%, a random guess. On the other hand, when  $r$  is large, the variance is small and the double descent phenomenon is mild or absent. Figure 2A shows a monotonically ascending test accuracy. In some extreme cases, for example when  $\gamma$  is small enough, the test accuracy continuously decreases after a very small ascent around  $\tau = 0$  (Figure 2D).

**3.2. Double descent in real dataset with practical GNNs.** Are these findings only relevant to the CSBM or they also occur with deeper GNNs on real datasets? We show in Figure 3 that they do. The effect is more pronounced for the loss than for the accuracy (although it does occur for both) which may explain why it is often hard to observe.

Figure 3 shows the results for two homophilic datasets, **Cora** and **Citeseer** [46], and two heterophilic datasets, **Chameleon** [42] and **Texas** [40], using different GCNs. We show the test loss (red) and the test accuracy (black) in node classification with different training ratios  $\tau$ . The primary source of variation between the different runs comes from the random train–test splits; model perturbations due to initialization are much smaller.

In the first column in Figure 3, we use a one-layer GCN similar to the one we analyzed theoretically but with added degree normalization, self-loops, and one-hot encoded labels as there are more than two classes. In **Cora** and **Citeseer**, the double descents of test risk and accuracy are both prominent. In **Texas**, which contains 183 nodes but has 1703 dimensional node feature, the test accuracy is almost monotonically decreasing, which is consistent with our theoretical model (Figure 2D).

In the second column of Figure 3, we use a two-layer GCN with ReLU activations and 16 neurons in the hidden layer. In the third column we add dropout. In the forth and fifth columns of Figure 3, we use the cross-entropy loss instead of the MSE, with dropout in the fifth. This last model is the same as the one in `pytorch-geometric` node classification tutorial<sup>2</sup>. While double descent still “survives” in the test loss on **Citeseer**, the test accuracy is almost monotonically increasing

<sup>2</sup><https://pytorch-geometric.readthedocs.io/en/latest/notes/colabs.html>

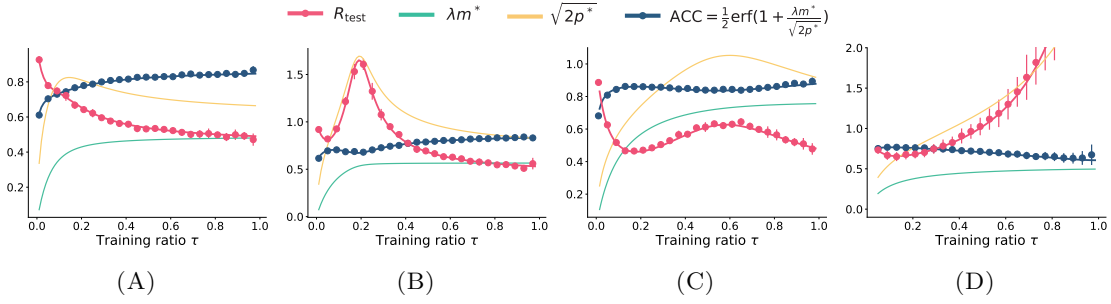


FIGURE 2. Four double descent curves. We show test accuracy and test risk for varying training ratios  $\tau$ . 2A: increasing ACC with large  $r$ ; 2B: double descent ACC with small  $r$ ; 2C: double descent ACC with  $\gamma$  close to 1; and 2D: (almost) decreasing ACC with small  $\gamma$ . We compare our theoretical results (solid line) with computer experiments (round dots) with  $\mathbf{P}(\mathbf{A}) = \mathbf{A}$  under different training ratios  $\tau$ . The parameters per columns are chosen as: 2A  $\mu = 1, \lambda = 2, \gamma = 5, r = 2$ ; 2B:  $\mu = 1, \lambda = 2, \gamma = 5, r = 0.1$ ; 2C:  $\mu = 1, \lambda = 2, \gamma = 1.2, r = 0.05$ ; 2D:  $\lambda = 1, \mu = 5, \gamma = 0.1, r = 0.005$ . We set  $N = 5000$  and  $d = 30$  for the first three plots, and  $N = 500$  and  $d = 20$  for the last plot. Each experimental data point is averaged over 10 independent trials and the standard deviation is indicated by vertical lines.

except on **Texas**. These results confirm the intuition that dropout and nonlinearity alleviate GNN overfitting on node classification, especially for large training ratios.

In the last row of Figure 3, we randomly remove 30% of the links and add the same number of random links. We also replace 30% of the entries in  $\mathbf{X}$  with the same number of random entries. Comparing the first row and the last row in Figure 3, we see that noisy datasets exhibit a much more prominent double descent which is consistent with our analysis. Beyond GCNs, we show that double descent occurs in more sophisticated GNNs like graph attention networks [50], GraphSAGE [19] and Chebyshev graph networks [8]; see Appendix E for details.

**3.3. Heterophily, homophily, and positive and negative self-loops.** The adjacency relation may encode very diverse semantics in different network-structured datasets. One way to characterize this is through the notions of homophily and heterophily. In a friendship graph links signify similarity: if Alice and Bob both know Jane it is reasonable to expect that Alice and Bob also know each other. This transitive relation results in *homophilic* graphs with preference for triangles (loops of length 3). On the other hand, in a protein interaction network, if proteins A and B interact, a small mutation A' of A will likely still interact with B but not with A. Thus “interaction” links signify partition and the corresponding heterophilic graphs have few triangles and a  $k$ -partite structure. Most networks are somewhere in between the homophilic and heterophilic extremes. A good synthetic model should then express both kinds of behavior: this is the case for CSBM where we can control the type of interactions through sign and magnitude of  $\lambda$ .

It has been empirically observed that graph neural networks often exhibit considerably worse performance on the heterophilic graphs than on homophilic graphs. There has been considerable activity in trying to understand this phenomenon as well as to mitigate it with special architectures and training strategies [7, 24, 27].

We show that this phenomenon can be understood by studying self-loops. Well-performing GCNs ubiquitously employ self-loops of the form  $\mathbf{P}(\mathbf{A}) = \mathbf{A} + \mathbf{I}_N$  which improve performance on homophilic datasets. But self-loops are not used for heterophilic datasets where they can often deteriorate performance. We compute the generalization error as a function of the self-loop intensity  $c$  in  $\mathbf{A} + c\mathbf{I}_N$ , but, crucially, also allowing negative values of  $c$  (see Appendix B). In Figure 5 we plot the test risk as a function of  $c$  for both positive and negative  $c$ . We find that a negative

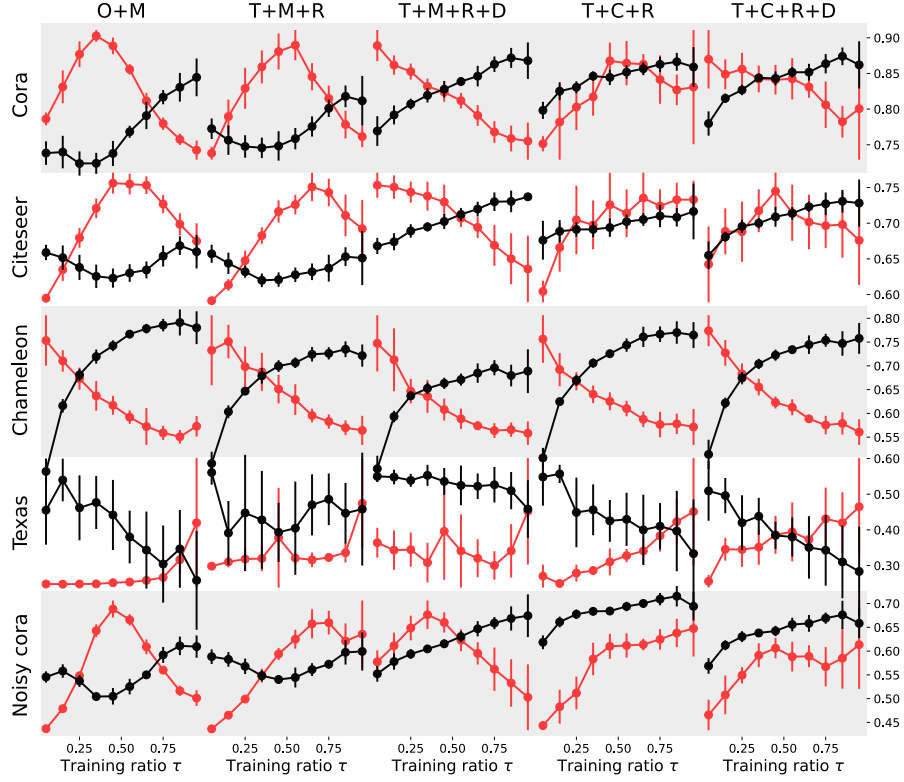


FIGURE 3. Double descent for different GNNs and datasets. We show test loss (red) and test accuracy (black) under different training ratios  $\tau$  on the abscissa, with different GCN settings, for 5 datasets, each in one row. **First column:** one linear layer (O) trained by MSE loss (M); **second column:** a two-layer GCN (T) with ReLU activations (R) and the MSE loss (M); **third column:** a two-layer GCN (T) with ReLU activation function (R), dropout (D), and MSE loss (M); **forth column:** a two-layer GCN (T) with ReLU activations (R) and cross-entropy loss (C); **fifth column:** T+C+R+D. Each experiemntal data point is averaged over 10 random test–train splits.

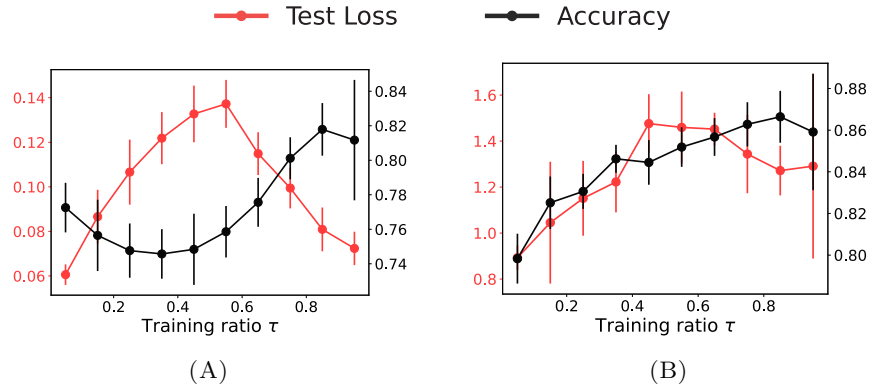


FIGURE 4. Double descents of the test loss (red) and test accuracy (black) on Cora under different training ratios  $\tau$  (abscissa) with a two-layer ReLU GCN. 4A: MSE loss; 4B: cross-entropy loss.



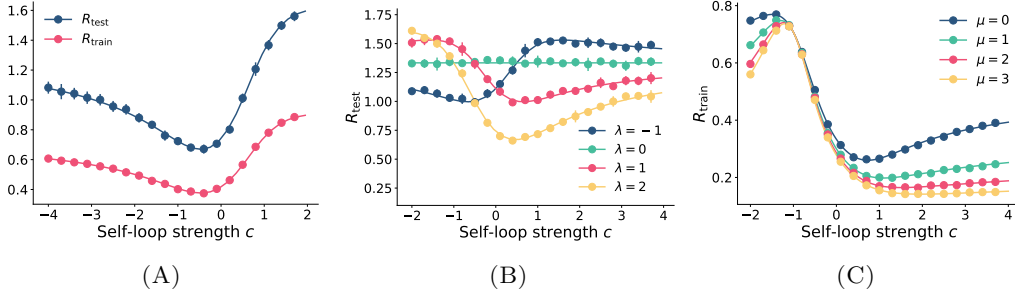


FIGURE 5. Risks on the CSBM with different self-loop intensity. 5A: training and test risk for  $\tau = 0.8$  and  $\lambda = -1$  (heterophilic). 5B: test risks for  $\gamma = 0.8$ ,  $\tau = 0.8$  and  $\mu = 0$  for different  $\lambda$ . 5C: training loss for different  $\mu$  when  $\tau = \lambda = 1$ . Each experimental data point is averaged over 10 independent trials with  $N = 5000$ ,  $r = 0$ , and  $d = 30$ . We use the non-symmetric binary adjacency matrix set  $\mathcal{A}^{\text{bn}}$ . The solid lines are the theoretical results from the replica method.

self-loop ( $c < 0$ ) results in much better performance on heterophilic data ( $\lambda < 0$ ). We sketch a signal-processing interpretation of this phenomenon in Appendix D.

**3.4. Positive and negative self-loops in real networks.** Remarkably, this finding also generalizes to more complicated graph neural networks and datasets. We experiment with two common heterophilic benchmarks, **Chameleon** and **Squirrel**, first with a two-layer ReLU GCN. The default GCN contains self-loops; we immediately observe in Figure 6 that removing them improves performance on both datasets. We then make the intensity of the self-loop adjustable as a hyper-parameter and find that a negative self-loop with  $c$  between  $-1.0$  and  $-0.5$  results in highest accuracy on both datasets. It is notable that the best performance in the two-layer ReLU GCN with  $c = -0.5$  (76.29%) is already close to state-of-the-art results by the Feature Selection Graph Neural Network (FSGNN) [29] (78.27%). FSGNN uses a graph filter bank  $\mathcal{B} = \{\mathbf{A}^k, (\mathbf{A} + \mathbf{I})^k\}$  with careful normalization. Taking a cue from the above findings, we show that a simple addition of negative self-loop filters  $(\mathbf{A} - 0.5\mathbf{I})^k$  to FSGNN yields the new state of the art (78.96%); see also Table 1.

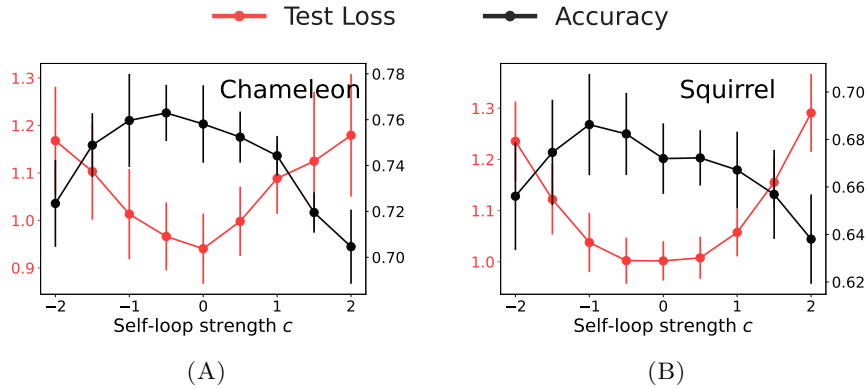


FIGURE 6. Node classification accuracy (black) and test loss (red) on real heterophilic graphs with different self-loop intensity on GCN. We implement a two-layer ReLU GCN with 128 hidden neurons and an additional self-loop with strength  $c$ . Every result is averaged over different training-test splits taken from [40] (60% training, 20% validation, 20% test). Standard deviation (vertical line) mainly comes from the randomness of the splits, yet the randomness of the model and optimizer is relatively small.

	GCN ( $c = 0$ )	GCN ( $c^*$ )	FSGNN	FSGNN ( $c^*$ )
<b>Chameleon</b>	75.81 $\pm$ 1.69	76.29 $\pm$ 1.22	78.27 $\pm$ 1.28	78.96 $\pm$ 1.05
<b>Squirrel</b>	67.19 $\pm$ 1.48	68.62 $\pm$ 2.13	74.10 $\pm$ 1.89	74.34 $\pm$ 1.21

TABLE 1. Comparison of test accuracy without and with the negative self-loop. The datasets and splits are the same as for Figure 6.

**3.5. Unsupervised vs semi-supervised vs fundamental limits.** An important interpretation of our results is that they quantify the value of labels in community detection. The results of Deshpande et al. indicate that when  $\mu^2/\gamma + \lambda^2 < 1$ , no unsupervised estimator can detect the latent structure  $\mathbf{y}$  from  $\mathbf{A}$  and  $\mathbf{X}$  [10]. Our analysis shows that even a small fraction of revealed labels allows us to break this barrier with a simple GCN. In Figure 7, we compare the accuracy of a one-layer GCN with unsupervised belief propagation (BP) [10]. We first run BP with  $\mu = \lambda = \gamma = 1$  and record the achieved accuracy. We then plot the smallest training ratio  $\tau$  for which the GCN achieves the same accuracy. We repeat this procedure for different feature SNRs  $\mu$  and graph SNRs  $\lambda$ . The dashed line indicates the information-theoretic threshold for detecting the latent structure from  $\mathbf{A}$  and  $\mathbf{X}$ .

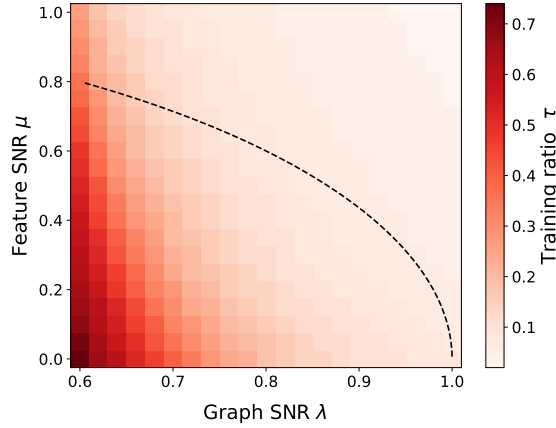


FIGURE 7. Training ratio at which a one-layer GCN matches performance of unsupervised belief propagation. The dashed line is the information-theoretic detection threshold when the data is  $(\mathbf{A}, \mathbf{X})$  but no labels are revealed.

#### 4. GENERALIZATION IN GCNs VIA STATISTICAL PHYSICS

The optimization problem (2) has a unique minimizer as long as  $r > 0$ . Since it is a least-squares problem linear in  $\mathbf{w}$ , we can write down a closed form solution,

$$(9) \quad \mathbf{w}^* = (r\mathbf{I}_F + (\mathbf{P}(\mathbf{A})\mathbf{X})^T \mathbf{I}_{\text{train}} \mathbf{P}(\mathbf{A})\mathbf{X})^{-1} (\mathbf{P}(\mathbf{A})\mathbf{X})^T \mathbf{I}_{\text{train}} \mathbf{y},$$

where

$$(\mathbf{I}_{\text{train}})_{ij} = \begin{cases} 1 & \text{if } i = j \in V_{\text{train}} \\ 0 & \text{otherwise.} \end{cases}$$

Analyzing generalization is in principle as simple as substituting the closed-form expression (9) into (3) and (4) and calculating the requisite averages. The procedure is however complicated by the interaction between the graph  $\mathbf{A}$  and the features  $\mathbf{X}$  and the fact that  $\mathbf{A}$  is a random binary adjacency matrix. Further, for a symmetric  $\mathbf{A}$ ,  $\mathbf{I}_{\text{train}} \mathbf{P}(\mathbf{A})$  is correlated with  $\mathbf{I}_{\text{test}} \mathbf{P}(\mathbf{A})$  even in a shallow GCN (and certainly in a deep one).

**4.1. The statistical physics program.** We interpret the (scaled) loss function as an energy, or a Hamiltonian,  $H(\mathbf{w}; \mathbf{A}, \mathbf{X}) = \tau N L_{\mathbf{A}, \mathbf{X}}(\mathbf{w})$ . Corresponding to this Hamiltonian is the Gibbs measure over the weights  $\mathbf{w}$ ,

$$d\mathbb{P}_\beta(\mathbf{w}; \mathbf{A}, \mathbf{X}) = \frac{\exp(-\beta H(\mathbf{w}; \mathbf{A}, \mathbf{X})) d\mathbf{w}}{Z_\beta(\mathbf{A}, \mathbf{X})} \quad \text{where} \quad Z_\beta(\mathbf{A}, \mathbf{X}) = \int d\mathbf{w} \exp(-\beta H(\mathbf{w}; \mathbf{A}, \mathbf{X})),$$

$\beta$  is the *inverse temperature* and  $Z_\beta$  is the *partition function*. At infinite temperature ( $\beta \rightarrow 0$ ), the Gibbs measure is diffuse; as temperature approaches zero ( $\beta \rightarrow \infty$ ), it converges to an atomic measure concentrated on the unique solution of (2),  $\mathbf{w}^* = \lim_{\beta \rightarrow \infty} \int \mathbf{w} \mathbb{P}_\beta(\mathbf{w}; \mathbf{A}, \mathbf{X}) d\mathbf{w}$ . In this latter case the partition function is similarly dominated by the minimum of the Hamiltonian. The expected loss can thus be computed from the *free energy density*  $f_\beta$ ,

$$\mathbb{E}_{\mathbf{A}, \mathbf{X}}[L_{\mathbf{A}, \mathbf{X}}(\mathbf{w}^*)] = -\frac{1}{\tau} \lim_{\beta \rightarrow \infty} f_\beta \quad \text{where} \quad f_\beta := -\lim_{N \rightarrow \infty} \frac{1}{N\beta} \mathbb{E}_{\mathbf{A}, \mathbf{X}} \ln Z_\beta(\mathbf{A}, \mathbf{X}).$$

Since the quenched average  $\mathbb{E} \ln Z_\beta$  is usually intractable, we apply the replica method [32] which allows us to take the expectation inside the logarithm and compute the annealed average,

$$\mathbb{E}_{\mathbf{A}, \mathbf{X}} \ln Z_\beta(\mathbf{A}, \mathbf{X}) = \lim_{n \rightarrow 0} \frac{\ln \mathbb{E}_{\mathbf{A}, \mathbf{X}} Z_\beta^n(\mathbf{A}, \mathbf{X})}{n}.$$

The gist of the replica method is to compute  $\mathbb{E}_{\mathbf{A}, \mathbf{X}} Z_\beta^n$  for integer  $n$  and then “pretend” that  $n$  is real and take the limit  $n \rightarrow 0$ . The computation for integer  $n$  is facilitated by the fact that  $Z_\beta^n$  normalizes the joint distribution of  $n$  independent copies of  $\mathbf{w}$ ,  $\{\mathbf{w}^a\}_{a=1}^n$ . We obtain

$$\begin{aligned} \mathbb{E}_{\mathbf{A}, \mathbf{X}} Z_\beta^n(\mathbf{A}, \mathbf{X}) &= \mathbb{E}_{\mathbf{A}, \mathbf{X}} (Z_\beta(\mathbf{A}, \mathbf{X}))_1 \times \cdots \times (Z_\beta(\mathbf{A}, \mathbf{X}))_n \\ (10) \quad &= \int \prod_{a=1}^n d\mathbf{w}^a \mathbb{E}_{\mathbf{A}, \mathbf{X}} \exp \left( \sum_{a=1}^n \left( -\beta \|\mathbf{I}_{\text{train}} \mathbf{A} \mathbf{X} \mathbf{w}^a - \mathbf{I}_{\text{train}} \mathbf{y}\|_2^2 \right) \right) \\ &\quad \times \exp(-\beta \tau r \|\mathbf{w}^a\|_2^2). \end{aligned}$$

Instead of working with the product  $\mathbf{A} \mathbf{X}$ , replica allows us to express the free energy density as a stationary point of a function where the dependence on  $\mathbf{A}$  and  $\mathbf{X}$  is separated (see Appendix A for details),

$$\begin{aligned} f_\beta &= \frac{1}{\beta} \text{extr} \lim_{n \rightarrow 0} \lim_{N \rightarrow \infty} \frac{1}{nN} (\mathbb{E}_{\mathbf{A}} [c(\mathbf{P}(\mathbf{A}))] + \mathbb{E}_{\mathbf{X}} [e(\mathbf{X})]) + D(m, p, q, \hat{m}, \hat{p}, \hat{q}) \\ (11) \quad &= \frac{1}{\beta} \text{extr}_{\substack{m, p, q \\ \hat{m}, \hat{p}, \hat{q}}} C(m, p, q) + E(\hat{m}, \hat{p}, \hat{q}) + D(m, p, q, \hat{m}, \hat{p}, \hat{q}), \end{aligned}$$

where we defined  $C \stackrel{\text{def}}{=} \frac{1}{nN} \mathbb{E}_{\mathbf{A}} [c(\mathbf{P}(\mathbf{A}))]$ ,  $E \stackrel{\text{def}}{=} \frac{1}{nN} \mathbb{E}_{\mathbf{X}} [e(\mathbf{X})]$ , which in the limit  $N \rightarrow \infty$ ,  $n \rightarrow 0$  only depend on the so-called order parameters  $m, p, q$  and  $\hat{m}, \hat{p}, \hat{q}$ . The separation thus allows us to study the influence of the distribution of  $\mathbf{A}$  in isolation; we provide the details in Appendix A.1. The risks (called the observables in physics) can be obtained from  $f_\beta$ .

**4.2. Gaussian adjacency equivalence.** A challenge in computing the quantities in (10) and (11) is to average over the binary adjacency matrix  $\mathbf{A}$ . We argue that  $f$  in (11) does not change if we instead average over the Gaussian ensemble with a correctly chosen mean and covariance. For a one-layer GCN ( $\mathbf{P}(\mathbf{A}) = \mathbf{A}$ ), we show that replacing  $\mathbb{E}_{\mathbf{A}^{\text{bs}}} c(\mathbf{P}(\mathbf{A}^{\text{bs}}))$  by  $\mathbb{E}_{\mathbf{A}^{\text{gn}}} c(\mathbf{P}(\mathbf{A}^{\text{gn}}))$  will not change  $f$  in (11) with  $\mathbf{A}^{\text{gn}}$  being a spiked non-symmetric Gaussian random matrix,

$$(12) \quad \mathbf{A}^{\text{gn}} = \frac{\lambda}{N} \mathbf{y} \mathbf{y}^T + \mathbf{\Xi}^{\text{gn}},$$

with  $\mathbf{\Xi}^{\text{gn}}$  having i.i.d. centered normal entries with variance  $1/N$ . This substitution is inspired by the universality results for the disorder of spin glasses [6, 39, 48] and the universality of mutual information in the CSBM [10]. Deshpande et al. [10] showed that the binary adjacency matrix in the stochastic block model can be replaced by

$$(13) \quad \mathbf{A}^{\text{gs}} = \frac{\lambda}{N} \mathbf{y} \mathbf{y}^T + \mathbf{\Xi}^{\text{gs}},$$

where  $\Xi^{\text{gs}} \in \mathbb{R}^{N \times N}$  is a sample from the standard Gaussian orthogonal ensemble, without affecting the mutual information between  $\mathbf{y}$  (which they modeled as random) and  $(\mathbf{A}, \mathbf{X})$  when  $N \rightarrow \infty$  and  $d \rightarrow \infty$ .

Our claim refers to certain averages involving  $\mathbf{A}$ ; we record it as a conjecture since our derivations are based on the non-rigorous replica method. We first define four probability distributions:

- (1)  $\mathcal{A}^{\text{bs}}$ : The distribution of adjacency matrices in the undirected CSBM (cf. (5)) scaled by  $1/\sqrt{d}$ ,  $\frac{1}{\sqrt{d}}\mathbf{A}^{\text{bs}} \sim \mathcal{A}^{\text{bs}}$ ;
- (2)  $\mathcal{A}^{\text{bn}}$ : the distribution of adjacency matrices in the directed CSBM (cf. (6)), scaled by  $1/\sqrt{d}$ ;
- (3)  $\mathcal{A}^{\text{gs}}$ : the distribution of spiked Gaussian orthogonal ensemble (cf. (13));
- (4)  $\mathcal{A}^{\text{gn}}$ : the distribution of spiked Gaussian random matrices (cf. (12)).

With these definitions in hand we can state

**Conjecture 1** (Equivalence of graph matrices). *Assume that  $d$  scales with  $N$  so that  $1/d \rightarrow 0$  and  $d/N \rightarrow 0$  when  $N \rightarrow \infty$ . Let  $\mathbf{P}(\mathbf{A})$  be a polynomial in  $\mathbf{A}$  used to define the GCN function in (1). It then holds that*

$$\begin{aligned} R_{\text{train}}(\mathcal{A}^{\text{b}\bullet}) &= R_{\text{train}}(\mathcal{A}^{\text{g}\bullet}), \\ R_{\text{test}}(\mathcal{A}^{\text{b}\bullet}) &= R_{\text{test}}(\mathcal{A}^{\text{g}\bullet}), \\ \text{ACC}(\mathcal{A}^{\text{b}\bullet}) &= \text{ACC}(\mathcal{A}^{\text{g}\bullet}), \end{aligned}$$

with  $\bullet \in \{\text{s}, \text{n}\}$ . When  $\mathbf{P}(\mathbf{A}) = \mathbf{A}$ , the values for symmetric and non-symmetric distributions also coincide.

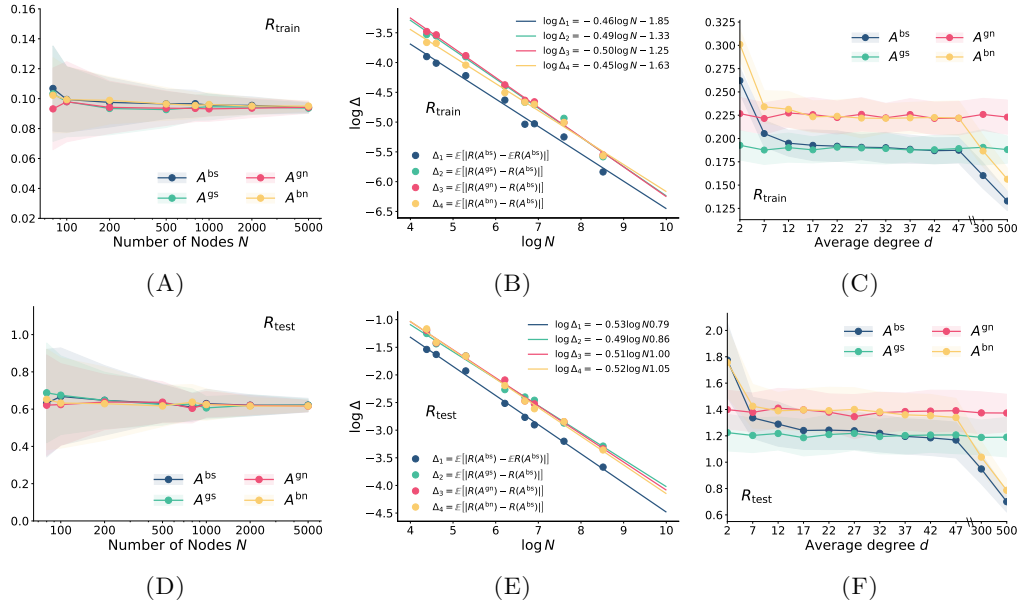


FIGURE 8. Experimental validation of Conjecture 1. In 8A & 8D: we show training and test risks with different numbers of nodes for  $\mathbf{P}(\mathbf{A}) = \mathbf{A}$ , with  $\gamma = \lambda = \mu = 2, r = 0.01, \tau = 0.8$  and  $d = \sqrt{N}/2$ . In 8B & 8E, we show the absolute values of difference between the risks with the binary and with the corresponding Gaussian adjacency, as a function of  $N$ , for data in 8A & 8D. We perform a linear regression on the data points with the logarithmic scale, and find that the error scales as  $|\Delta| \sim N^{-0.5}$ . In 8C & 8F we show the training and test risks for different average node degrees  $d$  and  $\mathbf{P}(\mathbf{A}) = \mathbf{A}^2$ .  $\lambda = \mu = 1, \gamma = 2$  and  $N = 2000$ . We set  $\gamma = 0.5, \tau = 0.8, r = 0.01$ .

In the case when  $\mathbf{P}(\mathbf{A}) = \mathbf{A}$  we justify Conjecture 1 by the replica method (see Appendix A). In the general case we provide abundant numerical evidence in Figure 8. We first consider the case when  $\mathbf{P}(\mathbf{A}) = \mathbf{A}$ . Figure 8A and Figure 8D show estimates of  $R_{\text{train}}$  and  $R_{\text{test}}$  averaged over 100 independent runs. The standard deviation over runs is indicated by the shading. We see that the means converge and the variance shrinks as  $N$  grows.

We also show absolute differences between the averages of  $R_{\text{train}}$  and  $R_{\text{test}}$  in Figure 8B and Figure 8E. We find that the values of  $R_{\text{train}}$  and  $R_{\text{test}}$  can be well fitted by a linear relationship in the logarithmic scale, suggesting that the absolute differences approach zero exponentially fast as  $N \rightarrow \infty$ . We next consider  $\mathbf{P}(\mathbf{A}) = \mathbf{A}^2$ . In Figure 8C and Figure 8F we can see that for intermediate values of  $d$ ,  $R_{\text{train}}$  and  $R_{\text{test}}$  corresponding to  $\mathbf{A}^{\text{bs}}$  and  $\mathbf{A}^{\text{bn}}$  are both close to that corresponding to  $\mathbf{A}^{\text{gs}}$  and  $\mathbf{A}^{\text{gn}}$ . This is consistent with the results shown in Figures 1 and 5 where the theoretical results computed by the replica method and  $\mathbf{A}^{\text{gn}}$  perfectly match the numerical results with  $\mathbf{A}^{\text{bn}}$  (for  $\mathbf{P}(\mathbf{A}) = \mathbf{A} + c\mathbf{I}_N$ ) and  $\mathbf{A}^{\text{bs}}$  (for  $\mathbf{P}(\mathbf{A}) = \mathbf{A}$ ), further validating the conjecture.

**4.3. Solution to the saddle point equation.** We can now solve the saddle point equation (11) by averaging over  $\mathbf{A}^{\text{gn}}$ . In the general case the solution is easy to obtain numerically. For an one-layer GCN with  $\mathbf{P}(\mathbf{A}) = \mathbf{A}$  we can compute a closed-form solution. Denoting the critical point in (11) by  $(m^*, p^*, q^*)$  we obtain

$$(14) \quad \begin{aligned} R_{\text{train}} &= \frac{(\lambda m^* - 1)^2 + p^*}{(2q^* + 1)^2}, \\ R_{\text{test}} &= (\lambda m^* - 1)^2 + p^*, \\ \text{ACC} &= \frac{1}{2} \left( 1 + \text{erf} \left( \frac{\lambda m^*}{\sqrt{2p^*}} \right) \right), \end{aligned}$$

where erf is the usual error function. While the general expressions are complicated (see Appendix A), in the ridgeless limit  $r \rightarrow 0$  we can compute simple closed-form expressions for train and test risks,

$$(15) \quad R_{\text{train}} = \frac{(\gamma + \mu)(\gamma\tau - 1)}{\gamma\tau(\gamma + \lambda^2(\mu + 1) + \mu)}, \quad R_{\text{test}} = \frac{\gamma\tau(\gamma + \mu)}{(\gamma\tau - 1)(\gamma + \lambda^2(\mu + 1) + \mu)},$$

assuming that  $\tau\gamma > 1$ .

**4.4. A rigorous solution.** It is worth noting that for a one-layer GCN risks can be computed rigorously using random matrix theory if we start with a Gaussian “adjacency matrix” instead of the true binary SBM adjacency matrix (following Conjecture 1). We outline this approach in Appendix C; in particular, for  $r = 0$ , the result of course coincides with that in (15).

## 5. DISCUSSION AND FURTHER WORK

We analyzed generalization in graph neural networks by making an analogy with a system of interacting particles. Earlier works modeled neurons in a neural network as particles; we let the particles correspond to the data points and the interactions be specified by the adjacency relation and the learnable weights. The latter can be interpreted as defining the “interaction physics” of the problem. The best weights correspond to the most plausible interaction physics, coupled in turn to the network formation mechanism.

Studying appropriate stylized models yields insights that are hard to get from complexity-based bounds of statistical learning theory. These bounds are often vacuous when in modern machine learning models. To wit, the authors of the PAC-Bayes analysis of generalization in GNNs [25] write that “[...] we are far from being able to explain the practical behaviors of GNNs.”

In contrast, we precisely traced the connection between generalization, the interaction type (homophilic or heterophilic) and the parameters of the GCN architecture and the dataset. We then showed that the learned lessons apply to a broad class of models and can be used constructively to improve performance of state-of-the-art graph neural networks on heterophilic data. Understanding the full picture will require advances in both learning-theory-based and physics-based analyses.

The setting that we analyzed is maybe the simplest combination of a graph convolution network and data distribution which exhibits interesting, realistic behavior. In order to capture a broader spectrum of complexity in graph learning we need to work on new ideas in random matrix theory and its neural network counterparts [41]. Regarding depth, while very deep GCNs are known to suffer from oversmoothing, there exists an interesting intermediate-depth regime [22]. Our techniques should apply simply by replacing  $\mathbf{A}$  by any polynomial  $\mathbf{P}(\mathbf{A})$  in (22), but we will need a generalization of existing random matrix theory results for HCIZ integrals. Finally, it is likely that these generalized results could be made fully rigorous if “universality” in Conjecture 1 could be established formally.

*Acknowledgments.* CS and ID were supported by the European Research Council (ERC) Starting Grant 852821—SWING. LP would like to acknowledge support from National Natural Science Foundation of China (NSFC) under Grant No. 62006122.

## REFERENCES

- [1] Aseem Baranwal, Kimon Fountoulakis, and Aukosh Jagannath, *Graph convolution for semi-supervised classification: Improved linear separability and out-of-distribution generalization*, arXiv preprint arXiv:2102.06966 (2021).
- [2] Jean Barbier, Nicolas Macris, and Cynthia Rush, *All-or-nothing statistical and computational phase transitions in sparse spiked matrix estimation*, Advances in Neural Information Processing Systems **33** (2020), 14915–14926.
- [3] Mikhail Belkin, Daniel Hsu, Siyuan Ma, and Soumik Mandal, *Reconciling modern machine-learning practice and the classical bias–variance trade-off*, Proceedings of the National Academy of Sciences **116** (2019), no. 32, 15849–15854.
- [4] Mikhail Belkin, Daniel Hsu, and Ji Xu, *Two models of double descent for weak features*, SIAM Journal on Mathematics of Data Science **2** (2020), no. 4, 1167–1180.
- [5] Stephen Boyd, Neal Parikh, Eric Chu, Borja Peleato, Jonathan Eckstein, et al., *Distributed optimization and statistical learning via the alternating direction method of multipliers*, Foundations and Trends® in Machine learning **3** (2011), no. 1, 1–122.
- [6] Philippe Carmona and Yueyun Hu, *Universality in sherrington–kirkpatrick’s spin glass model*, Annales de l’institut henri poincaré (b) probability and statistics, 2006, pp. 215–222.
- [7] Eli Chien, Jianhao Peng, Pan Li, and Olgica Milenkovic, *Adaptive universal generalized pagerank graph neural network*, arXiv preprint arXiv:2006.07988 (2020).
- [8] Michaël Defferrard, Xavier Bresson, and Pierre Vandergheynst, *Convolutional neural networks on graphs with fast localized spectral filtering*, Advances in neural information processing systems **29** (2016).
- [9] Yash Deshpande, Emmanuel Abbe, and Andrea Montanari, *Asymptotic mutual information for the balanced binary stochastic block model*, Information and Inference: A Journal of the IMA **6** (2017), no. 2, 125–170.
- [10] Yash Deshpande, Andrea Montanari, Elchanan Mossel, and Subhabrata Sen, *Contextual stochastic block models*, arXiv preprint arXiv:1807.09596 (2018).
- [11] Xiaowen Dong, Dorina Thanou, Laura Toni, Michael Bronstein, and Pascal Frossard, *Graph signal processing for machine learning: A review and new perspectives*, IEEE Signal processing magazine **37** (2020), no. 6, 117–127.
- [12] Thomas Dupic and Isaac Pérez Castillo, *Spectral density of products of wishart dilute random matrices. part i: the dense case*, arXiv preprint arXiv:1401.7802 (2014).
- [13] Ahmed El Alaoui and Michael I Jordan, *Detection limits in the high-dimensional spiked rectangular model*, Conference on learning theory, 2018, pp. 410–438.
- [14] Pascal Mattia Esser, Leena C Vankadara, and Debarghya Ghoshdastidar, *Learning theory can (sometimes) explain generalisation in graph neural networks*, 2021, pp. 14.
- [15] Joan Bruna Estrach, Wojciech Zaremba, Arthur Szlam, and Yann LeCun, *Spectral networks and deep locally connected networks on graphs*, 2nd international conference on learning representations, iclr, 2014.
- [16] Vikas K Garg, Stefanie Jegelka, and Tommi Jaakkola, *Generalization and representational limits of graph neural networks*, 2020, pp. 12.
- [17] Floris Geerts and Juan L Reutter, *Expressiveness and approximation properties of graph neural networks*, arXiv preprint arXiv:2204.04661 (2022).
- [18] Justin Gilmer, Samuel S Schoenholz, Patrick F Riley, Oriol Vinyals, and George E Dahl, *Neural message passing for quantum chemistry*, International conference on machine learning, 2017, pp. 1263–1272.
- [19] Will Hamilton, Zhitao Ying, and Jure Leskovec, *Inductive representation learning on large graphs*, Advances in neural information processing systems **30** (2017).
- [20] Mingguo He, Zhewei Wei, Hongteng Xu, et al., *Bernnet: Learning arbitrary graph spectral filters via bernstein approximation*, Advances in Neural Information Processing Systems **34** (2021), 14239–14251.
- [21] Hong Hu and Yue M Lu, *Universality laws for high-dimensional learning with random features*, arXiv preprint arXiv:2009.07669 (2020).

- [22] Nicolas Keriven, *Not too little, not too much: a theoretical analysis of graph (over) smoothing*, arXiv preprint arXiv:2205.12156 (2022).
- [23] Thomas N Kipf and Max Welling, *Semi-supervised classification with graph convolutional networks*, arXiv preprint arXiv:1609.02907 (2016).
- [24] Xiang Li, Renyu Zhu, Yao Cheng, Caihua Shan, Siqiang Luo, Dongsheng Li, and Weining Qian, *Finding global homophily in graph neural networks when meeting heterophily*, arXiv preprint arXiv:2205.07308 (2022).
- [25] Renjie Liao, Raquel Urtasun, and Richard Zemel, *A PAC-bayesian approach to generalization bounds for graph neural networks*, February 10, 2022.
- [26] Wei Lu, *Learning guarantees for graph convolutional networks on the stochastic block model*, International conference on learning representations, 2021.
- [27] Sitao Luan, Chenqing Hua, Qincheng Lu, Jiaqi Zhu, Mingde Zhao, Shuyuan Zhang, Xiao-Wen Chang, and Doina Precup, *Is heterophily a real nightmare for graph neural networks to do node classification?*, arXiv preprint arXiv:2109.05641 (2021).
- [28] Fragkiskos D Malliaros and Michalis Vazirgiannis, *Clustering and community detection in directed networks: A survey*, Physics reports **533** (2013), no. 4, 95–142.
- [29] Sunil Kumar Maurya, Xin Liu, and Tsuyoshi Murata, *Improving graph neural networks with simple architecture design*, arXiv preprint arXiv:2105.07634 (2021).
- [30] Miller McPherson, Lynn Smith-Lovin, and James M Cook, *Birds of a feather: Homophily in social networks*, Annual review of sociology (2001), 415–444.
- [31] Song Mei and Andrea Montanari, *The generalization error of random features regression: Precise asymptotics and the double descent curve*, Communications on Pure and Applied Mathematics **75** (2022), no. 4, 667–766.
- [32] Marc Mézard, Giorgio Parisi, and Miguel Angel Virasoro, *Spin glass theory and beyond: An introduction to the replica method and its applications*, Vol. 9, World Scientific Publishing Company, 1987.
- [33] Francesca Mignacco, Florent Krzakala, Yue Lu, Pierfrancesco Urbani, and Lenka Zdeborova, *The role of regularization in classification of high-dimensional noisy gaussian mixture*, International conference on machine learning, 2020, pp. 6874–6883.
- [34] Elchanan Mossel, Joe Neeman, and Allan Sly, *A proof of the block model threshold conjecture*, Combinatorica **38** (2018), no. 3, 665–708.
- [35] Preetum Nakkiran, Gal Kaplun, Yamini Bansal, Tristan Yang, Boaz Barak, and Ilya Sutskever, *Deep double descent: Where bigger models and more data hurt*, Journal of Statistical Mechanics: Theory and Experiment **2021** (2021), no. 12, 124003.
- [36] Kenta Oono and Taiji Suzuki, *Graph neural networks exponentially lose expressive power for node classification*, arXiv preprint arXiv:1905.10947 (2019).
- [37] Antonio Ortega, Pascal Frossard, Jelena Kovačević, José MF Moura, and Pierre Vandergheynst, *Graph signal processing: Overview, challenges, and applications*, Proceedings of the IEEE **106** (2018), no. 5, 808–828.
- [38] Samet Oymak, Christos Thrampoulidis, and Babak Hassibi, *The squared-error of generalized lasso: A precise analysis*, 2013 51st annual allerton conference on communication, control, and computing (allerton), 2013, pp. 1002–1009.
- [39] Dmitry Panchenko, *The sherrington-kirkpatrick model*, Springer Science & Business Media, 2013.
- [40] Hongbin Pei, Bingzhe Wei, Kevin Chen-Chuan Chang, Yu Lei, and Bo Yang, *Geom-gcn: Geometric graph convolutional networks*, arXiv preprint arXiv:2002.05287 (2020).
- [41] Jeffrey Pennington and Pratik Worah, *Nonlinear random matrix theory for deep learning*, Advances in neural information processing systems **30** (2017).
- [42] Benedek Rozemberczki, Carl Allen, and Rik Sarkar, *Multi-scale attributed node embedding*, Journal of Complex Networks **9** (2021), no. 2, cnab014.
- [43] Aliaksei Sandryhaila and José MF Moura, *Discrete signal processing on graphs*, IEEE transactions on signal processing **61** (2013), no. 7, 1644–1656.
- [44] Ryoma Sato, *A survey on the expressive power of graph neural networks*, arXiv preprint arXiv:2003.04078 (2020).
- [45] Franco Scarselli, Ah Chung Tsoi, and Markus Hagenbuchner, *The vapnik–chervonenkis dimension of graph and recursive neural networks* **108** (December 2018), 248–259.
- [46] Prithviraj Sen, Galileo Namata, Mustafa Bilgic, Lise Getoor, Brian Galligher, and Tina Eliassi-Rad, *Collective classification in network data*, AI magazine **29** (2008), no. 3, 93–93.
- [47] David I Shuman, Sunil K Narang, Pascal Frossard, Antonio Ortega, and Pierre Vandergheynst, *The emerging field of signal processing on graphs: Extending high-dimensional data analysis to networks and other irregular domains*, IEEE signal processing magazine **30** (2013), no. 3, 83–98.
- [48] Michel Talagrand, *Gaussian averages, bernoulli averages, and gibbs’ measures*, Random Structures & Algorithms **21** (2002), no. 3-4, 197–204.
- [49] Christos Thrampoulidis, Ehsan Abbasi, and Babak Hassibi, *Precise error analysis of regularized  $m$ -estimators in high dimensions*, IEEE Transactions on Information Theory **64** (2018), no. 8, 5592–5628.
- [50] Petar Velicković, Guillem Cucurull, Arantxa Casanova, Adriana Romero, Pietro Lio, and Yoshua Bengio, *Graph attention networks*, arXiv preprint arXiv:1710.10903 (2017).
- [51] Dan V Voiculescu, Ken J Dykema, and Alexandru Nica, *Free random variables*, American Mathematical Soc., 1992.

- [52] Xiyuan Wang and Muhan Zhang, *How powerful are spectral graph neural networks*, arXiv preprint arXiv:2205.11172 (2022).
- [53] Yuchung J Wang and George Y Wong, *Stochastic blockmodels for directed graphs*, Journal of the American Statistical Association **82** (1987), no. 397, 8–19.
- [54] Felix Wu, Amauri Souza, Tianyi Zhang, Christopher Fifty, Tao Yu, and Kilian Weinberger, *Simplifying graph convolutional networks*, International conference on machine learning, 2019, pp. 6861–6871.
- [55] Keyulu Xu, Weihua Hu, Jure Leskovec, and Stefanie Jegelka, *How powerful are graph neural networks?*, arXiv preprint arXiv:1810.00826 (2018).

## APPENDIX A. SKETCH OF THE DERIVATION

**A.1. Replica method.** We now outline the replica-based derivations. We first look at the one-layer GCN  $\mathbf{P}(\mathbf{A}) = \mathbf{A}$  for simplicity and to focus on the main idea. This corresponds to the training and test risks in (3). We extend the framework to self-loops in Appendix B.

We begin by defining the *augmented partition function*,

$$Z_\beta(\mathbf{A}, \mathbf{X}) = \int d\mathbf{w} \exp(-\beta H(\mathbf{w}) + t_0 \beta O_{\text{train}}(\mathbf{w}) + t_1 \beta O_{\text{test}}(\mathbf{w})),$$

where  $\beta$  is the inverse temperature, and the Hamiltonian

$$(16) \quad H(\mathbf{w}) = \|\mathbf{I}_{\text{train}} \mathbf{A} \mathbf{X} \mathbf{w} - \mathbf{I}_{\text{train}} \mathbf{y}\|_2^2 + \tau r \|\mathbf{w}\|_2^2$$

is the loss (2) scaled by  $N\tau$ . The “observables”  $O_{\text{train}}$  and  $O_{\text{test}}$  are the quantities we are interested in—the (scaled) training and test risks,

$$O_{\text{train}}(\mathbf{w}) = \|\mathbf{I}_{\text{train}} \mathbf{A} \mathbf{X} \mathbf{w} - \mathbf{I}_{\text{train}} \mathbf{y}\|_2^2, \quad O_{\text{test}}(\mathbf{w}) = \|\mathbf{I}_{\text{test}} \mathbf{A} \mathbf{X} \mathbf{w} - \mathbf{I}_{\text{test}} \mathbf{y}\|_2^2.$$

When the inverse temperature  $\beta$  is small, the Gibbs measure  $Z_\beta^{-1}(\mathbf{A}, \mathbf{X}) \exp(-\beta H(\mathbf{w})) d\mathbf{w}$  is diffuse; when  $\beta \rightarrow \infty$ , the Gibbs measure converges to an atomic measure concentrated on the unique solution of (2). That is to say, for  $t_0 = t_1 = 0$ , we can write

$$\mathbf{w}^* = \lim_{\beta \rightarrow \infty} \int \mathbf{w} \mathbb{P}_\beta(\mathbf{w}; \mathbf{A}, \mathbf{X}) d\mathbf{w}, \quad \text{where} \quad \mathbb{P}_\beta(\mathbf{w}; \mathbf{A}, \mathbf{X}) = \frac{1}{Z_\beta(\mathbf{A}, \mathbf{X})} \exp(-\beta H(\mathbf{w})).$$

The idea is to compute the values of the observables in the large system limit at a finite temperature and then consider their values as  $\beta \rightarrow \infty$ . To this end, we define the *free energy density*  $f_\beta$  corresponding to the augmented partition function,

$$(17) \quad f_\beta := - \lim_{N \rightarrow \infty} \frac{1}{N\beta} \mathbb{E}_{\mathbf{A}, \mathbf{X}} \ln Z_\beta(\mathbf{A}, \mathbf{X}).$$

The expected risks can be computed as

$$(18) \quad R_{\text{train}} = \frac{1}{\tau} \lim_{\beta \rightarrow \infty} \left. \frac{\partial f_\beta}{\partial t_0} \right|_{t_0=0, t_1=0}, \quad R_{\text{test}} = \frac{1}{1-\tau} \lim_{\beta \rightarrow \infty} \left. \frac{\partial f_\beta}{\partial t_1} \right|_{t_0=0, t_1=0}.$$

Although  $\ln Z_\beta(\mathbf{A}, \mathbf{B})/N$  concentrates for large  $N$ , a direct computation of the quenched average (17) is intractable. We now use the *replica trick* which transforms the quenched average into an average where the expectation is inside the logarithm,

$$(19) \quad \mathbb{E}_{\mathbf{A}, \mathbf{X}} \ln Z_\beta(\mathbf{A}, \mathbf{X}) = \lim_{n \rightarrow 0} \frac{\ln \mathbb{E}_{\mathbf{A}, \mathbf{X}} Z_\beta^n(\mathbf{A}, \mathbf{X})}{n}.$$

The main idea of the replica method is to first compute  $\mathbb{E}_{\mathbf{A}, \mathbf{X}} Z_\beta^n$  for integer  $n$  by interpreting  $Z_\beta^n = (Z_\beta)_1 (Z_\beta)_2 \dots (Z_\beta)_n$  as the product of  $n$  partition functions for  $n$  independent configurations  $\{\mathbf{w}^a\}_{a=1}^n$ . We then obtain  $\mathbb{E}_{\mathbf{A}, \mathbf{X}} \ln Z_\beta$  by taking the limit  $n \rightarrow 0$  in (19) even though the expression of  $\ln \mathbb{E}_{\mathbf{A}, \mathbf{X}} Z_\beta^n$  is only valid for integer  $n$ . We have

$$(20) \quad \begin{aligned} \mathbb{E}_{\mathbf{A}, \mathbf{X}} Z_\beta^n(\mathbf{A}, \mathbf{X}) &= \mathbb{E}_{\mathbf{A}, \mathbf{X}} (Z_\beta(\mathbf{A}, \mathbf{X}))_1 \times \dots \times (Z_\beta(\mathbf{A}, \mathbf{X}))_n \\ &= \int \prod_{a=1}^n d\mathbf{w}^a \mathbb{E}_{\mathbf{A}, \mathbf{X}} \exp \left( \sum_{a=1}^n \left( -\|\mathbf{I}_\beta \mathbf{A} \mathbf{X} \mathbf{w}^a - \mathbf{I}_\beta \mathbf{y}\|_2^2 \right) \right) \exp(-\beta \tau r \|\mathbf{w}^a\|_2^2), \end{aligned}$$

where we defined  $\mathbf{I}_\beta \stackrel{\text{def}}{=} \sqrt{\beta - \beta t_0} \mathbf{I}_{\text{train}} + \sqrt{-\beta t_1} \mathbf{I}_{\text{test}}$ . We first fix  $\mathbf{X}$  and take the expectation over  $\mathbf{A}$ . Directly computing the expectation over the binary graph matrix  $\mathbf{A} \sim \mathcal{A}^{\text{bs}}$  is non-trivial.



To make progress, we average over  $\mathbf{A} \sim \mathcal{A}^{\text{gn}}$  (instead cf. (12)). In Appendix A.2 we show that this Gaussian substitution does not change the free energy density, ultimately yielding the same risks and accuracies as detailed in Conjecture 1.

Letting  $\boldsymbol{\sigma}^a = \mathbf{X}\mathbf{w}^a$ , the vector  $\mathbf{A}^{\text{gn}}\boldsymbol{\sigma}^a$  is now jointly Gaussian for any fixed  $\boldsymbol{\sigma}^a$  and  $C = \frac{1}{nN} \ln \mathbb{E}_{\mathbf{A}} \exp \left( \sum_{a=1}^n \left( -\|\mathbf{I}_{\beta}\mathbf{A}\boldsymbol{\sigma}^a - \mathbf{I}_{\beta}\mathbf{y}\|_2^2 \right) \right)$  can be computed by multivariate Gaussian integration. It is not hard to see that  $C$  depends only on a vector  $\mathbf{m} \in \mathbb{R}^n$  and a matrix  $\mathbf{Q} \in \mathbb{R}^{n \times n}$  defined as

$$(21) \quad \mathbf{m}_a = \mathbf{y}^T \boldsymbol{\sigma}^a / N, \quad \text{and} \quad \mathbf{Q}_{ab} = (\boldsymbol{\sigma}^a)^T \boldsymbol{\sigma}^b / N.$$

In statistical physics these quantities are called the *order parameters*. We then define

$$(22) \quad \begin{aligned} C(\mathbf{m}, \mathbf{Q}) &= \frac{1}{nN} \ln \mathbb{E}_{\mathbf{A}} c(\mathbf{A}) \\ &= \frac{1}{nN} \ln \mathbb{E}_{\mathbf{A}} \exp \left( - \sum_a \|\mathbf{I}_{\beta}\mathbf{A}\boldsymbol{\sigma}^a - \mathbf{I}_{\beta}\mathbf{y}\|_2^2 \right). \end{aligned}$$

Using the identity  $\delta(t - t_0) = \frac{1}{2\pi} \int d\omega \exp(i\omega(t - t_0))$  we can write

$$(23) \quad \begin{aligned} \delta(N\mathbf{Q}_{ab} - (\mathbf{w}^a)^T \mathbf{X}^T \mathbf{X} \mathbf{w}^b) &= \frac{1}{2\pi} \int d\hat{\mathbf{Q}}_{ab} \exp \left( i\hat{\mathbf{Q}}_{ab} (N\mathbf{Q}_{ab} - (\mathbf{w}^a)^T \mathbf{X}^T \mathbf{X} \mathbf{w}^b) \right) \\ \delta(N\mathbf{m}_a - \mathbf{y}^T \mathbf{X} \mathbf{w}^a) &= \frac{1}{2\pi} \int d\hat{\mathbf{m}}_a \exp \left( i\hat{\mathbf{m}}_a (N\mathbf{m}_a - \mathbf{y}^T \mathbf{X} \mathbf{w}^a) \right), \end{aligned}$$

so that (20) becomes

$$(24) \quad \begin{aligned} \mathbb{E}_{\mathbf{A}, \mathbf{X}} Z_{\beta}^n(\mathbf{A}, \mathbf{X}) &= \left( \frac{iN}{2\pi} \right)^{\frac{n^2+3n}{2}} \int \prod_{a \leq b} d\mathbf{Q}_{ab} \prod_{a \leq b} d\hat{\mathbf{Q}}_{ab} \prod_a d\mathbf{m}_a \prod_a d\hat{\mathbf{m}}_a \\ &\times \exp(nNC(\mathbf{m}, \mathbf{Q})) \times \exp \left( nNE(\hat{\mathbf{m}}, \hat{\mathbf{Q}}) \right) \\ &\times \exp \left( N \sum_{a \leq b} \hat{\mathbf{Q}}_{ab} \mathbf{Q}_{ab} + N \sum_a \hat{\mathbf{m}}_a \mathbf{m}_a \right), \end{aligned}$$

where

$$(25) \quad \begin{aligned} E(\hat{\mathbf{m}}, \hat{\mathbf{Q}}) &= \frac{1}{nN} \ln \mathbb{E}_{\mathbf{X}} e(\mathbf{X}) \\ &= \frac{1}{nN} \ln \mathbb{E}_{\mathbf{X}} \int \prod_{a=1}^n d\mathbf{w}_a \exp \left( - \sum_{a \leq b} \hat{\mathbf{Q}}_{ab} (\mathbf{w}^a)^T \mathbf{X}^T \mathbf{X} \mathbf{w}^b \right. \\ &\quad \left. - \sum_a \hat{\mathbf{m}}_a \mathbf{y}^T \mathbf{X} \mathbf{w}^a - \tau r \beta \sum_a \|\mathbf{w}_a\|_2^2 \right). \end{aligned}$$

In (24) and (25), we apply the change of variables  $i\mathbf{Q}_{ab} \rightarrow \mathbf{Q}_{ab}$ ,  $i\mathbf{m}_a \rightarrow \mathbf{m}_a$ . Note that while (22) still depends on  $\mathbf{X}$ , we do not average over it. As  $\mathbf{A}$  and  $\mathbf{X}$  appear as a product in (19), it is not straightforward to average over them simultaneously. We average over  $\mathbf{A}$  first to arrive at (24), and then find that (22)-(25) are self-averaging, meaning that they concentrate around their expectation as  $N \rightarrow \infty$ . Ultimately, this allows us to isolate the randomness in  $\mathbf{A}$  and  $\mathbf{X}$ . It also opens the possibility to adapt our framework to other graph filters by simply replacing  $\mathbf{A}$  by  $\mathbf{P}(\mathbf{A})$  in (22). Since (2) has a unique solution, we can leverage the replica symmetry assumption which yields

$$(26) \quad \mathbf{m} = m\mathbf{1}_n, \quad \hat{\mathbf{m}} = \hat{m}\mathbf{1}_n, \quad \mathbf{Q} = q\mathbf{I}_n + p\mathbf{1}_n\mathbf{1}_n^T, \quad \text{and} \quad \hat{\mathbf{Q}} = \hat{q}\mathbf{I}_n + \hat{p}\mathbf{1}_n\mathbf{1}_n^T.$$

In the limit  $N \rightarrow \infty$ ,  $n \rightarrow 0$ , we are only interested in the leading order contributions to  $C(\mathbf{m}, \mathbf{Q})$  so we write (with a small abuse of notation),

$$(27) \quad \begin{aligned} C(m, p, q) = & \frac{\tau (2\beta(1-t_0)q + \lambda m)^2}{2q(2\beta(1-t_0)q + 1)} - \beta(1-t_0)\tau - \frac{\tau}{2} \frac{2\beta(1-t_0)p}{2\beta(1-t_0)q + 1} - \frac{\tau \lambda^2 m^2}{2q} \\ & + \frac{(1-\tau)(-2t_1q + \lambda m)^2}{2q(-2t_1 + 1)} + t_1(1-\tau) - \frac{(1-\tau)}{2} \frac{-2t_1p}{-2t_1q + 1} \\ & - \frac{(1-\tau)\lambda^2 m^2}{2q} + o(1) + \beta o_\beta(1).^3 \end{aligned}$$

Similarly,

$$(28) \quad E(\hat{m}, \hat{p}, \hat{q}) = \frac{1}{2(2\hat{q} + \hat{p})\gamma} \left( \hat{p}(1 - \hat{r}T) + \gamma \hat{m}^2 \left( 1 - \frac{T\hat{r} + \gamma - 1}{T^2\mu\hat{r} + (\gamma - 1)T\mu + \gamma} \right) \right) + o(1) + \beta o_\beta(1),$$

where

$$(29) \quad T = \frac{1}{2\hat{r}} \left( 1 - \hat{r} - \gamma + \sqrt{1 + \hat{r}^2 + 2\hat{r} + 2\gamma\hat{r} - 2\gamma + \gamma^2} \right) \quad \text{and} \quad \hat{r} = \frac{2\tau r}{2\hat{q} + \hat{p}}.$$

We give the details of the derivation of  $C$  in Appendix A.2 and of  $E$  in Appendix A.3.

When  $r \rightarrow 0$ , we have  $T \rightarrow \frac{1}{1-\gamma}$ , and

$$(30) \quad E(\hat{m}, \hat{p}, \hat{q}) = \frac{1}{2} \left( \frac{\hat{m}^2}{2\hat{q} + \hat{p}} \right) \left( \frac{\mu + 1}{\gamma + \mu} \right) - \frac{1}{2\gamma} \frac{\hat{p}}{(2\hat{q} + \hat{p})} + o(1).$$

We can now compute (24) by integrating over only 6 variables:  $m$ ,  $\hat{m}$ ,  $q$ ,  $\hat{q}$ ,  $p$ , and  $\hat{p}$ . For  $N \rightarrow \infty$ , the integral can be computed via the saddle point method. We get

$$(31) \quad f_\beta = \frac{1}{\beta} \text{extr}_{m, \hat{m}, q, \hat{q}, p, \hat{p}} \lim_{n \rightarrow 0} \lim_{N \rightarrow \infty} C(m, p, q) + E(\hat{m}, \hat{p}, \hat{q}) + (q + p)(\hat{q} + \hat{p}) - \frac{1}{2} p\hat{p} + m\hat{m}.$$

The stationary point is a solution of

$$(32) \quad \frac{\partial f_\beta}{\partial m} = \frac{\partial f_\beta}{\partial \hat{m}} = \frac{\partial f_\beta}{\partial p} = \frac{\partial f_\beta}{\partial \hat{p}} = \frac{\partial f_\beta}{\partial q} = \frac{\partial f_\beta}{\partial \hat{q}} = 0.$$

When  $\beta \rightarrow \infty$ , the stationary point only exists if  $m, \hat{m}, p, \hat{p}, q, \hat{q}$  scale as

$$p = \mathcal{O}(1), \quad q = \mathcal{O}\left(\frac{1}{\beta}\right), \quad \hat{p} = \mathcal{O}(\beta^2), \quad 2\hat{q} + \hat{p} = \mathcal{O}(\beta), \quad m = \mathcal{O}(1), \quad \hat{m} = \mathcal{O}(\beta).$$

We thus reparameterize as

$$p \rightarrow p, \quad \beta q \rightarrow q, \quad \frac{\hat{p}}{\beta^2} \rightarrow \hat{p}, \quad \frac{1}{\beta} (2\hat{q} + \hat{p}) \rightarrow \hat{q}, \quad m \rightarrow m, \quad \frac{1}{\beta} \hat{m} \rightarrow \hat{m}.$$

Ignoring the small terms which vanish when  $n \rightarrow 0, N \rightarrow \infty, \beta \rightarrow \infty$ , and denoting  $f = \lim_{\beta \rightarrow \infty} f_\beta$ , we get

$$(33) \quad \begin{aligned} f = & \text{extr}_{m, \hat{m}, q, \hat{q}, p, \hat{p}} g(t_0 - 1, \tau) + g(t_1, 1 - \tau) + \frac{1}{2} (\hat{q}p + q\hat{p} + 2m\hat{m}) \\ & + \frac{1}{2} \frac{\hat{m}^2}{\hat{q}} \left( 1 - \frac{T\hat{r} + \gamma - 1}{T^2\mu\hat{r} + (\gamma - 1)T\mu + \gamma} \right) - \frac{1}{2\gamma} \frac{\hat{p}(1 - \hat{r}T)}{\hat{q}}, \end{aligned}$$

where

$$g(t, \tau) = t\tau - \frac{\tau t p}{2tq + 1} - \frac{\tau \lambda^2 m^2}{2q} + \frac{\tau (2tq + \lambda m)^2}{2q(2tq + 1)},$$

and  $\hat{r} = \frac{2\tau r}{\hat{q}}$ . Denote by  $m^*, p^*, q^*, \hat{m}^*, \hat{p}^*, \hat{q}^*$  the stationary point in (33). Substituting into (18) yields the risks in 14.

<sup>3</sup>We use the asymptotic notation  $o(1)$  for deterministic and random quantities which vanish in the limit  $n \rightarrow 0, N \rightarrow \infty$  in a suitable sense. We similarly use  $o_\beta(1)$  in the limit  $\beta \rightarrow \infty$ . The order parameters  $m, p, q$  in (27) as well as  $\hat{m}, \hat{p}, \hat{q}$  in (30) scale in  $\beta$  or a polynomial of  $\beta$ .

To get an expression for the accuracy, we study the order parameters. Because  $\mathbf{w}^*$  is the unique solution in (2), and considering the definition of order parameters (21), stationarity in (33) implies that

$$(34) \quad \begin{aligned} p^* &= \lim_{N \rightarrow \infty} \mathbb{E}_{\mathbf{A}, \mathbf{X}} \left[ \mathbf{w}^{*T} \mathbf{X}^T \mathbf{X} \mathbf{w}^* / N \right], \\ m^* &= \lim_{N \rightarrow \infty} \mathbb{E}_{\mathbf{A}, \mathbf{X}} \left[ \mathbf{y}^T \mathbf{X} \mathbf{w}^* / N \right]. \end{aligned}$$

Let  $\mathbf{A}_{\text{train}} \in \mathbb{R}^{F \times N}$  be the selection of rows from  $\mathbf{A}$  corresponding to  $i$ -th row for all  $i \in V_{\text{train}}$  and  $\mathbf{A}_{\text{test}} \in \mathbb{R}^{(N-F) \times N}$  be the selection of rows corresponding to  $i$ -th row for all  $i \in V_{\text{test}}$ . The network output for the test nodes reads  $\mathbf{h}_{\text{test}} = \mathbf{A}_{\text{test}} \boldsymbol{\sigma}^*$ , where  $\boldsymbol{\sigma}^* = \mathbf{X} \mathbf{w}^*$ . Since we work with a non-symmetric Gaussian random matrix  $\mathbf{A} \sim \mathcal{A}^{\text{gn}}$  as our graph matrix, the  $\mathbf{A}_{\text{test}}$  are independent of  $\mathbf{A}_{\text{train}}$  and  $\boldsymbol{\sigma}^*$  (Note  $\boldsymbol{\sigma}^* = \mathbf{X} \mathbf{w}^*$  depends on  $\mathbf{A}_{\text{train}}$ ). Therefore, for any fixed  $\mathbf{A}_{\text{train}}$  and  $\mathbf{X}$  but random  $\mathbf{A}_{\text{test}}$ , the network output for test nodes is jointly Gaussian,

$$\mathbf{A}_{\text{test}} \boldsymbol{\sigma}^* \sim \mathcal{N} \left( \frac{\lambda \mathbf{y}^T \boldsymbol{\sigma}^*}{N} \mathbf{y}, (\boldsymbol{\sigma}^*)^T \boldsymbol{\sigma}^* I_N \right).$$

Combining this with (34), we obtain the test accuracy as

$$(35) \quad \text{ACC} = \mathbb{P}(x > 0), \quad \text{where } x \sim \mathcal{N}(\lambda m^*, p^*) > 0.$$

**A.2. Computation of  $C(\cdot)$ .** Recalling (22) we define

$$(36) \quad G(\mathcal{A}) := \frac{1}{nN} \ln \mathbb{E}_{\mathbf{A} \sim \mathcal{A}} c(\mathbf{A}).$$

We begin by computing  $G(\mathcal{A}^{\text{gn}}) = C(m, p, q)$  in (27) where  $\mathcal{A}^{\text{gn}}$  denotes the distribution of non-symmetric Gaussian spiked matrices (12). We then show that the symmetry does not influence its value, i.e.,  $G(\mathcal{A}^{\text{gn}})/\beta = G(\mathcal{A}^{\text{gs}})/\beta$  when  $N, d, \beta \rightarrow \infty$  and  $d/N, n \rightarrow 0$ . Finally, we show that the Gaussian substitution for the binary adjacency matrix does not influence the corresponding free energy density, which ultimately leads to the same risks and accuracies under different adjacency matrices (Conjecture 1).

We concatenate  $\{\boldsymbol{\sigma}^a\}_{a=1}^n$  as

$$\tilde{\boldsymbol{\sigma}} = [(\boldsymbol{\sigma}^1)_1, \dots, (\boldsymbol{\sigma}^a)_1, \dots, (\boldsymbol{\sigma}^n)_1, (\boldsymbol{\sigma}^1)_2, \dots, (\boldsymbol{\sigma}^a)_2, \dots, (\boldsymbol{\sigma}^n)_2, \dots, (\boldsymbol{\sigma}^n)_N]^T.$$

Then we rewrite (36) as

$$(37) \quad G(\mathcal{A}) = \frac{1}{nN} \ln \mathbb{E}_{\mathbf{A}} \exp \left( - \left\| ((\mathbf{I}_\beta \mathbf{A}) \otimes \mathbf{1}_n) \tilde{\boldsymbol{\sigma}} - (\mathbf{I}_\beta \mathbf{y}) \otimes \mathbf{1}_n \right\|_2^2 \right),$$

where  $\otimes$  is the Kronecker product. By the central limit theorem, when  $N \rightarrow \infty$ , the vectors  $(\mathbf{A} \otimes \mathbf{1}_n) \tilde{\boldsymbol{\sigma}}$  for  $\mathbf{A} \sim \mathcal{A}^{\text{gn}}$ ,  $\mathbf{A} \sim \mathcal{A}^{\text{bn}}$ ,  $\mathbf{A} \sim \mathcal{A}^{\text{gs}}$  and  $\mathbf{A} \sim \mathcal{A}^{\text{bs}}$  all converge in distribution to jointly Gaussian random vectors. Letting  $\boldsymbol{\mu}(\mathcal{A})$  and  $\boldsymbol{\Sigma}(\mathcal{A})$  be the mean and the covariance of  $\mathbf{A} \sim \mathcal{A}$ , we obtain

$$(38) \quad \begin{aligned} G(\mathcal{A}) &= \frac{1}{nN} \left( \ln \frac{1}{\sqrt{\det(\mathbf{I}_{nN} + 2\mathbf{I}_{n\beta}^2 \boldsymbol{\Sigma}(\mathcal{A}))}} - \frac{1}{2} \boldsymbol{\mu}^T(\mathcal{A}) \boldsymbol{\Sigma}^{-1}(\mathcal{A}) \boldsymbol{\mu}(\mathcal{A}) - (\mathbf{y} \otimes \mathbf{1}_n)^T \mathbf{I}_{n\beta}^2 (\mathbf{y} \otimes \mathbf{1}_n) \right. \\ &\quad + \left( \frac{1}{2} (2(\mathbf{y} \otimes \mathbf{1}_n)^T \mathbf{I}_{n\beta}^2 + \boldsymbol{\mu}^T(\mathcal{A}) \boldsymbol{\Sigma}^{-1}(\mathcal{A})) (\boldsymbol{\Sigma}^{-1}(\mathcal{A}) + 2\mathbf{I}_{n\beta}^2)^{-1} \right. \\ &\quad \left. \left. \times (2\mathbf{I}_{n\beta}^2 \mathbf{y} \otimes \mathbf{1}_n + \boldsymbol{\Sigma}^{-1}(\mathcal{A}) \boldsymbol{\mu}(\mathcal{A})) \right) \right) + o(1) \end{aligned}$$

where  $\mathbf{I}_{n\beta} = \mathbf{I}_\beta \otimes \mathbf{I}_n$ . The vanishing lower-order term  $o(1)$  comes from the tails in the central limit theorem and it is thus absent when  $\mathcal{A} = \mathcal{A}^{\text{gn}}$ . In this case we have

$$(39) \quad \boldsymbol{\mu}(\mathcal{A}^{\text{gn}}) = \lambda \mathbf{y} \otimes \mathbf{m}, \quad \boldsymbol{\Sigma}(\mathcal{A}^{\text{gn}}) = \mathbf{I}_N \otimes \mathbf{Q},$$

with  $\mathbf{m}$  and  $\mathbf{Q}$  defined in (21). Leveraging the replica symmetric assumption (26), we compute the determinant term in (38) as

$$\begin{aligned}
(40) \quad \frac{1}{nN} \det(\mathbf{I}_{nN} + 2\mathbf{I}_{n\beta}^2 \Sigma(\mathcal{A}^{\text{gn}})) &= \tau \ln(2\beta(1-t_0)q+1) + \tau \frac{2\beta(1-t_0)np}{2\beta(1-t_0)q+1} \\
&\quad + (1-\tau) \ln(2(-\beta t_1)q+1) + (1-\tau) \frac{2(-\beta t_1)p}{2(-\beta t_1)q+1} \\
&= \tau \frac{2\beta(1-t_0)p}{2\beta(1-t_0)q+1} + (1-\tau) \frac{2(-\beta t_1)p}{2(-\beta t_1)q+1} + o(1) \\
&\quad + \tau \ln(2\beta(1-t_0)q+1) + (1-\tau) \ln(2(-\beta t_1)q+1).
\end{aligned}$$

The  $o(1)$  in the second equality comes from the approximation  $\frac{1}{n} \ln(1+n) = 1 + o(1)$ . The last two terms in (40) do not increase with  $\beta$  and can thus be neglected in the limit  $\beta \rightarrow \infty$  when computing  $G(\mathcal{A})/\beta$ ; they give rise to  $\beta o_\beta(1)$  in (27). We compute the remaining terms in (38) as

$$\begin{aligned}
\frac{1}{2nN} \boldsymbol{\mu}(\mathcal{A}^{\text{gn}})^\top \Sigma^{-1}(\mathcal{A}^{\text{gn}}) \boldsymbol{\mu}(\mathcal{A}^{\text{gn}}) &= \frac{\lambda^2 m^2}{2q} + o(1) \\
\frac{1}{nN} (\mathbf{y} \otimes \mathbf{1}_n)^\top \mathbf{I}_{n\beta}^2 (\mathbf{y} \otimes \mathbf{1}_n) &= \tau\beta(1-t_0) + (1-\tau)(-\beta t_1), \\
\frac{1}{nN} \times \text{last two lines in (38)} &= \tau \frac{(2\beta(1-t_0)q + \lambda m)^2}{2q(1+2\beta(1-t_0)q)} + (1-\tau) \frac{(2(-\beta t_1)q + \lambda m)^2}{2q(1+2(-\beta t_1)q)} + o(1).
\end{aligned}$$

Collecting everything we get  $G(\mathcal{A}^{\text{gn}})$  in (27). Note that  $G(\mathcal{A}^{\text{gn}})/\beta = \mathcal{O}(1)$ , and we are going to show that  $G(\mathcal{A}^{\text{gn}})/\beta - G(\mathcal{A}^{\text{gs}})/\beta = o(1)$ .

For  $\mathcal{A}^{\text{gs}}$ ,  $\mathcal{A}^{\text{bn}}$  and  $\mathcal{A}^{\text{bs}}$ , we find the means and covariances of  $(\mathbf{A} \otimes \mathbf{1}_n) \tilde{\boldsymbol{\sigma}}$  as

$$\begin{aligned}
(41) \quad \boldsymbol{\mu}(\mathcal{A}^{\text{gs}}) &= \boldsymbol{\mu}(\mathcal{A}^{\text{gn}}), & \Sigma(\mathcal{A}^{\text{gs}}) &= \Sigma(\mathcal{A}^{\text{gn}}) + \frac{1}{N} \tilde{\boldsymbol{\sigma}}^\top \tilde{\boldsymbol{\sigma}} \\
\boldsymbol{\mu}(\mathcal{A}^{\text{bn}}) &= \boldsymbol{\mu}(\mathcal{A}^{\text{gn}}) + \sqrt{d} \mathbf{1}_N \otimes \mathbf{l}, & \Sigma(\mathcal{A}^{\text{bn}}) &= \Sigma(\mathcal{A}^{\text{gn}}) \left( 1 + \mathcal{O}\left(\frac{1}{\sqrt{d}} + \frac{d}{N}\right) \right) \\
\boldsymbol{\mu}(\mathcal{A}^{\text{bs}}) &= \boldsymbol{\mu}(\mathcal{A}^{\text{gn}}) + \sqrt{d} \mathbf{1}_N \otimes \mathbf{l}, & \Sigma(\mathcal{A}^{\text{bs}}) &= \Sigma(\mathcal{A}^{\text{gn}}) \left( 1 + \mathcal{O}\left(\frac{1}{\sqrt{d}} + \frac{d}{N}\right) \right) \\
&& &+ \frac{1 + \mathcal{O}\left(\frac{1}{\sqrt{d}} + \frac{d}{N}\right)}{N} \tilde{\boldsymbol{\sigma}}^\top \tilde{\boldsymbol{\sigma}},
\end{aligned}$$

where  $\mathbf{l} \in \mathbb{R}^n$  with entries  $\mathbf{l}_a = \frac{\mathbf{1}_N^\top \boldsymbol{\sigma}^a}{N}$  are also order parameters similarly to  $\mathbf{m}$  (21). Substituting (41) into (38), we see that the perturbation  $\frac{1}{N} \tilde{\boldsymbol{\sigma}}^\top \tilde{\boldsymbol{\sigma}}$  in  $\Sigma(\mathcal{A}^{\text{gs}})$  leads to a  $\mathcal{O}(\frac{1}{N})$  perturbation in  $G(\mathcal{A}^{\text{gs}})$ , while the perturbation of  $\mathcal{O}\left(\frac{1}{\sqrt{d}} + \frac{d}{N}\right)$  in  $\Sigma(\mathcal{A}^{\text{bn}})$  and  $\Sigma(\mathcal{A}^{\text{bs}})$  leads to a  $\mathcal{O}(\frac{1}{\sqrt{d}} + \frac{d}{N})$  perturbation in  $G(\mathcal{A})$ .

In  $\boldsymbol{\mu}(\mathcal{A}^{\text{bn}})$  and  $\boldsymbol{\mu}(\mathcal{A}^{\text{gn}})$ , there is a bias  $\mathbf{l}$ . By the replica symmetric assumption (26), we have  $\mathbf{l} = \mathbf{l} \mathbf{1}_n$ . It is possible to show that a critical point in the saddle point equation (31) exists only when  $\mathbf{l} = 0$  for  $\beta \rightarrow \infty$ . Therefore, the term  $\sqrt{d} \mathbf{1}_N \otimes \mathbf{l}$  will not influence the value of free energy density when  $\beta \rightarrow \infty$ . It further implies that the elements of  $\boldsymbol{\sigma}^* = \mathbf{X} \mathbf{w}^*$  are symmetrically distributed around zero. This is analogous to the vanishing average magnetization for the Sherrington-Kirkpatrick model [32].

To summarize this section, as long as  $\frac{1}{N}, \frac{1}{\sqrt{d}}, \frac{d}{N} \rightarrow 0$ , averaging over  $\mathcal{A}^{\text{bs}}$ ,  $\mathcal{A}^{\text{gn}}$ ,  $\mathcal{A}^{\text{gs}}$  and  $\mathcal{A}^{\text{gn}}$  is equivalent in (31) with  $\beta \rightarrow \infty$  for a one-layer GCN with  $\mathbf{P}(\mathbf{A}) = \mathbf{A}$ .<sup>4</sup>

<sup>4</sup>In general it does not hold that  $G(\mathcal{A}^{\text{gn}}) = G(\mathcal{A}^{\text{bn}})$  nor that  $G(\mathcal{A}^{\text{gs}}) = G(\mathcal{A}^{\text{bs}})$ . The equivalence stems from the fact that  $\boldsymbol{\sigma}^* = \mathbf{X} \mathbf{w}^*$  are symmetrically distributed, but for any fixed  $\boldsymbol{\sigma}^*$  with  $\mathbf{l} = \mathbf{1}_N^\top \boldsymbol{\sigma}^* \neq 0$ , we have  $G(\mathcal{A}^{\text{gn}}) = G(\mathcal{A}^{\text{bn}}) + l^2 \mathcal{O}(1)$  and  $G(\mathcal{A}^{\text{gs}}) = G(\mathcal{A}^{\text{bs}}) + l^2 \mathcal{O}(1)$ .

A.3. **Computation of  $E$ .** Recalling (25) and denoting  $\bar{\mathbf{Q}} = \hat{\mathbf{Q}} + \text{diag}(\hat{\mathbf{Q}})$ , we have

$$(42) \quad E(\hat{\mathbf{m}}, \hat{\mathbf{Q}}) = \frac{1}{nN} \ln \mathbb{E}_{\mathbf{X}} \sqrt{\frac{(2\pi)^{nN}}{\det(\mathbf{X}^\top \mathbf{X} \otimes \bar{\mathbf{Q}} + 2\tau r \beta \mathbf{I}_{nF})}} \\ \times \exp \left( \frac{1}{2} \left( \mathbf{y}^\top \mathbf{X} \otimes \hat{\mathbf{M}}^\top \right) (\mathbf{X}^\top \mathbf{X} \otimes \bar{\mathbf{Q}} + 2\tau r \beta \mathbf{I}_{nF})^{-1} \left( \mathbf{X}^\top \mathbf{y} \otimes \hat{\mathbf{M}} \right) \right).$$

Because the determinant term and the exponential term in (42) are both self-averaging when  $N \rightarrow \infty$ , we can compute them separately.

Denoting by  $\lambda_f(\mathbf{X}^\top \mathbf{X})$  the  $f$ -th largest eigenvalue of  $\mathbf{X}^\top \mathbf{X}$ , we have

$$(43) \quad \frac{1}{nN} \ln \left( \sqrt{\frac{(2\pi)^{nN}}{\det(\mathbf{X}^\top \mathbf{X} \otimes \hat{\mathbf{Q}} + 2\tau r \beta \mathbf{I}_{nF})}} \right) \\ = - \frac{\hat{p}}{2\gamma(2\hat{q} + \hat{p})} \left( 1 - \sum_f^F \frac{1}{F} \frac{2\tau r \beta / (2\hat{q} + \hat{p})}{\lambda_f + 2\tau r \beta / (2\hat{q} + \hat{p})} \right) \\ + \frac{1}{2\gamma} \log(2\pi) - \frac{1}{F} \frac{n}{2\gamma} \sum_{f=1}^F \log((2\hat{q} + \hat{p}) \lambda_f + 2\tau r \beta) + o(1)$$

For the same reasons as in (40), the two logarithmic terms in the last line of (43) can be ignored since they do not grow in the scale of  $\beta$ . To compute the first term in the RHS of (43), using the shortcut  $\hat{r} \stackrel{\text{def}}{=} 2\tau r \beta / (2\hat{q} + \hat{p})$ , we get

$$(44) \quad T(\hat{r}, \gamma) = \frac{1}{\hat{r}} \sum_f^F \frac{1}{F} \frac{\hat{r}}{\lambda_f + \hat{r}} \\ = \frac{1}{2\hat{r}} \left( 1 - \hat{r} + \sqrt{1 + \hat{r}^2 + 2\hat{r} + 2\gamma\hat{r} - 2\gamma + \gamma^2 - \gamma} \right) + o(1),$$

which is obtained by integrating over the Marchenko–Pastur distribution.

The exponential term in (42) can be computed as

$$\begin{aligned} & \frac{1}{2nN} \left( \mathbf{y}^\top \mathbf{X} \otimes \hat{\mathbf{m}}^\top \right) (\mathbf{X}^\top \mathbf{X} \otimes \bar{\mathbf{Q}} + 2\tau r \beta \mathbf{I}_{nF})^{-1} (\mathbf{X}^\top \mathbf{y} \otimes \hat{\mathbf{m}}) \\ &= \frac{1}{2nN} \left( \mathbf{y}^\top \mathbf{X} \otimes \hat{\mathbf{m}}^\top \right) (\mathbf{X}^\top \mathbf{X} \otimes (\bar{\mathbf{Q}} - p \mathbf{1}_n \mathbf{1}_n^\top) + 2\tau r \beta \mathbf{I}_{nF})^{-1} (\mathbf{X}^\top \mathbf{y} \otimes \hat{\mathbf{m}}) + o(1) \\ &= \frac{1}{2nN} \left( \hat{\mathbf{m}}^\top (\bar{\mathbf{Q}} - p \mathbf{1}_n \mathbf{1}_n^\top)^{-1} \hat{\mathbf{m}} \right) \left( \mathbf{y}^\top \mathbf{X} (\mathbf{X}^\top \mathbf{X} + \hat{r} \mathbf{I}_F)^{-1} \mathbf{X}^\top \mathbf{y} \right) + o(1) \\ &= \frac{1}{2} \frac{\hat{m}^2}{2\hat{q} + \hat{p}} \left( 1 - \frac{T\hat{r} + \gamma - 1}{T^2 \mu \hat{r} + (\gamma - 1) T \mu + \gamma} \right) + o(1), \end{aligned}$$

in which we first perturb  $\bar{\mathbf{Q}}$  by  $p \mathbf{1}_n \mathbf{1}_n^\top$  in the second line and then compute  $\left( \mathbf{y}^\top \mathbf{X} (\mathbf{X}^\top \mathbf{X} + \hat{r} \mathbf{I}_F)^{-1} \mathbf{X}^\top \mathbf{y} \right)$  by the Woodbury matrix identity.

## APPENDIX B. SELF-LOOP COMPUTATION

When  $\mathbf{P}(\mathbf{A}) = \mathbf{A} + c \mathbf{I}_N$ , we still follow the replica pipeline from Section A but with different, more complicated  $C$  and  $E$  in (24).

B.1.  **$C$  with self-loop.** We replace  $\mathbf{A}$  by  $\mathbf{A} + c \mathbf{I}_N$  in (22). Now the expectation over  $\mathbf{A}$  is not only a function of  $\mathbf{m}$  and  $\mathbf{Q}$ , but also of

$$(45) \quad (\mathbf{m}^0)_a = \frac{1}{N} \mathbf{y}^\top \mathbf{I}_{\text{train}} \boldsymbol{\sigma}^a, \quad (\mathbf{m}^1)_a = \frac{1}{N} \mathbf{y}^\top \mathbf{I}_{\text{test}} \boldsymbol{\sigma}^a, \\ (\mathbf{Q}^0)_{ab} = \frac{1}{N} (\boldsymbol{\sigma}^a)^\top \mathbf{I}_{\text{train}} \boldsymbol{\sigma}^b, \quad (\mathbf{Q}^1)_{ab} = \frac{1}{N} (\boldsymbol{\sigma}^a)^\top \mathbf{I}_{\text{test}} \boldsymbol{\sigma}^b.$$

For  $\mathbf{A} \sim \mathcal{A}^{\text{gn}}$ , since  $((\mathbf{A} + c\mathbf{I}_N) \otimes \mathbf{1}_n)\tilde{\boldsymbol{\sigma}}$  is jointly Gaussian with mean and covariance

$$\boldsymbol{\mu}(\mathcal{A}^{\text{gn}}) = \lambda \mathbf{y} \otimes \mathbf{m} + c\tilde{\boldsymbol{\sigma}}, \quad \boldsymbol{\Sigma}(\mathcal{A}^{\text{gn}}) = \mathbf{I}_N \otimes \mathbf{Q},$$

we can compute (38) directly. Leveraging the replica symmetric assumption, i.e.,

$$\begin{aligned} \mathbf{m}^0 &= m_0 \mathbf{1}_n & \mathbf{m}^1 &= m_1 \mathbf{1}_n \\ \mathbf{Q}^0 &= q_0 \mathbf{I}_n + p_0 \mathbf{1}_n \mathbf{1}_n^\top & \mathbf{Q}^1 &= q_1 \mathbf{I}_n + p_1 \mathbf{1}_n \mathbf{1}_n^\top, \end{aligned}$$

we have

$$\begin{aligned} C(\mathbf{m}^0, \mathbf{m}^1, \mathbf{Q}^0, \mathbf{Q}^1) &= \tau \frac{(2\beta_0 q + \lambda m)^2}{q(1 + 2\beta_0 q)} + (1 - \tau) \frac{(2\beta_1 q + \lambda m)^2}{q(1 + 2\beta_1 q)} \\ &\quad + c^2 \frac{(1 + 2\beta_0 q) p_0 q - (1 + 4\beta_0 q) p q_0}{q^2 (1 + 2\beta_0 q)^2} + c^2 \frac{(1 + 2\beta_1 q) p_1 q - (1 + 4\beta_1 q) p q_1}{q^2 (1 + 2\beta_1 q)^2} \\ &\quad + 2c \left( \frac{\lambda m + 2\beta_0 q}{q(1 + 2\beta_0 q)} m_0 + \frac{\lambda m + 2\beta_1 q}{q(1 + 2\beta_1 q)} m_1 \right) + o(1) + o_\beta(1). \end{aligned}$$

where  $\beta_0 = \beta(1 - t_0)$ ,  $\beta_1 = -\beta t_1$ ,  $q = q_0 + q_1$ ,  $m = m_0 + m_1$  and  $p = p_0 + p_1$ .

**B.2.  $E$  with self-loop.** After applying the Fourier representation method (23) to the new order parameters (45), we obtain new dual variables  $\widehat{\mathbf{m}}^0, \widehat{\mathbf{m}}^1, \widehat{\mathbf{Q}}^0, \widehat{\mathbf{Q}}^1$ . We then rewrite (25) as

$$\begin{aligned} E(\widehat{\mathbf{m}}^0, \widehat{\mathbf{m}}^1, \widehat{\mathbf{Q}}^0, \widehat{\mathbf{Q}}^1) &= \frac{1}{nN} \ln \mathbb{E}_{\mathbf{X}} \int \prod_{a=1}^n d\mathbf{w}_a \exp \left( - \sum_{a \leq b} (\widehat{\mathbf{Q}}^0)_{ab} (\mathbf{w}^a)^\top \mathbf{X}^\top \mathbf{I}_{\text{train}} \mathbf{X} \mathbf{w}^b - \sum_a (\widehat{\mathbf{m}}^0)_a \mathbf{y}^\top \mathbf{X} \mathbf{I}_{\text{train}} \mathbf{w}^a \right. \\ &\quad \left. - \sum_{a \leq b} (\widehat{\mathbf{Q}}^1)_{ab} (\mathbf{w}^a)^\top \mathbf{X}^\top \mathbf{I}_{\text{test}} \mathbf{X} \mathbf{w}^b - \sum_a (\widehat{\mathbf{m}}^1)_a \mathbf{y}^\top \mathbf{X} \mathbf{I}_{\text{test}} \mathbf{w}^a - \tau r \beta \sum_a \|\mathbf{w}^a\|_2^2 \right). \end{aligned}$$

Integrating over  $\mathbf{w}_a$  yields

$$\begin{aligned} (46) \quad E &= \frac{1}{nN} \ln \mathbb{E}_{\mathbf{X}} \sqrt{\frac{(2\pi)^{nN}}{\det(\mathbf{X}^\top \mathbf{I}_{\text{train}} \mathbf{X} \otimes \bar{\mathbf{Q}}^0 + \mathbf{X}^\top \mathbf{I}_{\text{test}} \mathbf{X} \otimes \bar{\mathbf{Q}}^1 + 2\tau r \beta \mathbf{I}_{nF})}} \\ &\quad \times \exp \left( \frac{1}{2} \left( \mathbf{y}^\top \otimes (\widehat{\mathbf{m}}^0)^\top \mathbf{I}_{\text{train}} \mathbf{X} + \mathbf{y}^\top \mathbf{I}_{\text{test}} \mathbf{X} \otimes (\widehat{\mathbf{m}}^1)^\top \right) \right. \\ &\quad \left. \times \left( \mathbf{X}^\top \mathbf{I}_{\text{train}} \mathbf{X} \otimes \bar{\mathbf{Q}}^0 + \mathbf{X}^\top \mathbf{I}_{\text{test}} \mathbf{X} \otimes \bar{\mathbf{Q}}^1 + 2\tau r \beta \mathbf{I}_{nF} \right)^{-1} \left( \mathbf{X}^\top \mathbf{I}_{\text{train}} \mathbf{y} \otimes \widehat{\mathbf{m}}^0 + \mathbf{X}^\top \mathbf{I}_{\text{test}} \mathbf{y} \otimes \widehat{\mathbf{m}}^1 \right) \right), \end{aligned}$$

where  $\bar{\mathbf{Q}}^0 = \widehat{\mathbf{Q}}^0 + \text{diag}(\widehat{\mathbf{Q}}^0)$  and  $\bar{\mathbf{Q}}^1 = \widehat{\mathbf{Q}}^1 + \text{diag}(\widehat{\mathbf{Q}}^1)$ . By replica symmetry, we have

$$(47) \quad \begin{aligned} \widehat{\mathbf{m}}^0 &= \widehat{m}_0 \mathbf{1}_n & \widehat{\mathbf{m}}^1 &= \widehat{m}_1 \mathbf{1}_n \\ \bar{\mathbf{Q}}_0 &= \widehat{q}_0 \mathbf{I}_n + \widehat{p}_0 \mathbf{1}_n \mathbf{1}_n^\top & \bar{\mathbf{Q}}_1 &= \widehat{q}_1 \mathbf{I} + \widehat{p}_1 \mathbf{1}_n \mathbf{1}_n^\top. \end{aligned}$$

Similarly as in Appendix A.3, because the determinant term and the exponential term are both self-averaging when  $N \rightarrow \infty$ , we compute them separately. For the sake of simplicity we only consider  $r = 0$  and  $\mu = 0$  in what follows. Denoting  $\mathbf{Y}^0 = \mathbf{X}^\top \mathbf{I}_{\text{train}} \mathbf{X}$  and  $\mathbf{Y}^1 = \mathbf{X}^\top \mathbf{I}_{\text{test}} \mathbf{X}$ , we write the determinant term in (46) in the replica limit as

$$\begin{aligned} (48) \quad &\lim_{n \rightarrow 0} \frac{1}{nN} \ln \det(\mathbf{Y}^0 \otimes \bar{\mathbf{Q}}^0 + \mathbf{Y}^1 \otimes \bar{\mathbf{Q}}^1) \\ &= \lim_{n \rightarrow 0} \frac{1}{nN} \ln \left( \mathbf{I}_F + n(\widehat{p}_0 \mathbf{Y}^0 + \widehat{p}_1 \mathbf{Y}^1) (\widehat{q}_0 \mathbf{Y}^0 + \widehat{q}_1 \mathbf{Y}^1)^{-1} \right) (\widehat{q}_0 \mathbf{Y}^0 + \widehat{q}_1 \mathbf{Y}^1)^n \\ &= \frac{1}{N} \text{Tr}(\widehat{p}_0 \mathbf{Y}^0 + \widehat{p}_1 \mathbf{Y}^1) (\widehat{q}_0 \mathbf{Y}^0 + \widehat{q}_1 \mathbf{Y}^1)^{-1}. \end{aligned}$$

The exponential term in (46) can be computed similarly, noting that  $\mathbf{Y}^0$  and  $\mathbf{Y}^1$  are rotationally invariant since  $\mu = 0$ ,

$$(49) \quad \begin{aligned} & \exp \left\{ \frac{1}{2} \left( \mathbf{y}^\top \mathbf{I}_{\text{train}} \mathbf{X} \otimes (\widehat{\mathbf{m}}^0)^\top + \mathbf{y}^\top \mathbf{I}_{\text{test}} \mathbf{X} \otimes (\widehat{\mathbf{m}}^1)^\top \right) \left( \mathbf{X}^\top \mathbf{I}_{\text{train}} \mathbf{X} \otimes \bar{\mathbf{Q}}^0 + \mathbf{X}^\top \mathbf{I}_{\text{test}} \mathbf{X} \otimes \bar{\mathbf{Q}}^1 \right)^{-1} \right. \\ & \quad \left. \times \left( \mathbf{X}^\top \mathbf{I}_{\text{train}} \mathbf{y} \otimes \widehat{\mathbf{m}}^0 + \mathbf{X}^\top \mathbf{I}_{\text{test}} \mathbf{y} \otimes \widehat{\mathbf{m}}^1 \right) \right\} \\ & = \exp \left\{ \text{Tr} \left( n (\widehat{q}_0 \mathbf{Y}^0 + \widehat{p}_1 \mathbf{Y}^1) (\widehat{m}_0^2 \mathbf{Y}^0 + \widehat{m}_1^2 \mathbf{Y}^1)^{-1} \right) \right\}, \end{aligned}$$

Both (48) and (49) involve the same quantity,

$$(50) \quad \begin{aligned} U(a, b, c, d) & \stackrel{\text{def}}{=} \mathbb{E}_{\mathbf{X}} \left[ \text{Tr} \left( (a \mathbf{Y}^0 + b \mathbf{Y}^1) (c \mathbf{Y}^0 + d \mathbf{Y}^1)^{-1} \right) \right] \\ & = \frac{a}{c} \mathbb{E}_{\mathbf{X}} \left[ \text{Tr} \left( \mathbf{Y}^0 \left( \mathbf{Y}^0 + \frac{d}{c} \mathbf{Y}^1 \right)^{-1} \right) \right] + \frac{b}{d} \mathbb{E}_{\mathbf{X}} \left[ \text{Tr} \left( \mathbf{Y}^1 \left( \frac{c}{d} \mathbf{Y}^0 + \mathbf{Y}^1 \right)^{-1} \right) \right], \end{aligned}$$

which can be computed by random matrix free convolution [51]. The Green's function (also called the Cauchy function in the mathematical literature) is defined via the Stieltjes transform

$$(51) \quad G_{\mathbf{Y}}(z) := \int \frac{\rho_{\mathbf{Y}}(\lambda)}{z - \lambda} d\lambda = \frac{1}{N} \text{Tr} (z \mathbf{I}_N - \mathbf{Y})^{-1},$$

which in turn yields the spectrum transform  $\rho_{\mathbf{Y}}(\lambda) = -\frac{1}{\pi} \lim_{\epsilon \rightarrow 0} \Im G_{\mathbf{Y}}(z) \big|_{z=\lambda+i\epsilon}$ . The corresponding Voiculescu S-transform reads

$$S_{\mathbf{Y}}(w) = \frac{1+w}{w} \chi(w) \quad \text{where} \quad \frac{1}{\chi(w)} G_{\mathbf{Y}} \left( \frac{1}{\chi(w)} \right) - 1 = w \quad \text{and} \quad \frac{1}{\chi(w)} = z.$$

We then get the multiplicative free convolution as

$$(52) \quad S_{\mathbf{Y}^0 \mathbf{Y}^1}(w) = S_{\mathbf{Y}^0}(w) S_{\mathbf{Y}^1}(w).$$

After computing  $S_{\mathbf{Y}^0(\mathbf{Y}^1)^{-1}}$  and  $S_{\mathbf{Y}^1(\mathbf{Y}^0)^{-1}}$ , we obtain the expression for  $U$  in (50). For example, for  $\tau = 0.8$  and  $\gamma = 5$ , the eigenvalue distributions of  $\mathbf{Y}_0, \mathbf{Y}_1$  asymptotically follow the Marchenko-Pastur distribution,

$$\rho_{\mathbf{Y}^0}(\lambda) = \frac{\sqrt{16 - \lambda}}{8\pi\sqrt{\lambda}} \mathbb{1}_{\lambda \in \{1,9\}}, \quad \rho_{\mathbf{Y}^1}(\lambda) = \frac{\sqrt{4 - \lambda}}{2\pi\sqrt{\lambda}} \mathbb{1}_{\lambda \in \{0,1\}}.$$

We then get that

$$(53) \quad U(a, b, c, d) = -\frac{aF - \frac{2d}{c} + \sqrt{9 + \frac{16d}{c}} - 3}{c \cdot \frac{2d}{c}(\frac{d}{c} - 1)} - \frac{bF}{d} \frac{5 - \sqrt{\frac{9c+16}{\frac{d}{c}}}}{-\frac{2c}{d} + 2}.$$

Once  $C$  and  $E$  are computed, we have all the ingredients of the saddle point equation (31) with 12 variables,

$$m_0, m_1, \widehat{m}_0, \widehat{m}_1, p_0, p_1, \widehat{p}_0, \widehat{p}_1, q_0, q_1, \widehat{q}_0 \quad \text{and} \quad \widehat{m}_1.$$

A critical point of this saddle point equation gives the explicit formulas for the risks in Section A.

#### APPENDIX C. A RANDOM MATRIX THEORY APPROACH

As mentioned in Section 4, if we start with the Gaussian adjacency matrices defined before Conjecture 1 we can obtain some of the results described above. For simplicity, we outline this approach for the full observation case  $\mathbf{I}_{\text{train}} = \mathbf{I}_N$ , that is, for  $\tau = 1$ , and compute the empirical risk. The partial observation case follows the same strategy but involves more complicated calculations. We let  $\alpha \stackrel{\text{def}}{=} \frac{1}{\gamma} = \frac{F}{N}$ , and rescale variables as  $\sqrt{\mu\gamma} \rightarrow \mu$ ,  $\sqrt{F}u \rightarrow u$ . Following Conjecture 1,

we replace the binary symmetric adjacency matrix  $\mathbf{A}^{\text{bs}}$  by the Gaussian random matrix with a rank-one spike so that

$$\begin{aligned}\mathbf{A} &= \Xi^{\text{gn}} + \frac{\lambda}{N} \mathbf{y} \mathbf{y}^\top, \\ \mathbf{X} &= \Xi^x + \frac{\mu}{N} \mathbf{y} \mathbf{u}^\top.\end{aligned}$$

The ridge loss reads,

$$L(\mathbf{w}) = \frac{1}{N} \|\mathbf{y} - \mathbf{A} \mathbf{X} \mathbf{w}\|_2^2 + \frac{r}{N} \|\mathbf{w}\|^2,$$

and has the unique minimizer

$$\begin{aligned}\mathbf{w}^* &= \arg \min_{\mathbf{w}} L(\mathbf{w}) \\ &= (r \mathbf{I}_F + \mathbf{X}^\top \mathbf{A}^\top \mathbf{A} \mathbf{X})^{-1} \mathbf{X}^\top \mathbf{A}^\top \\ &= (r \mathbf{I}_F + \Phi^\top \Phi)^{-1} \Phi^\top \mathbf{y},\end{aligned}$$

with  $\Phi = \mathbf{A} \mathbf{X}$ . Our target is to compute the empirical risk,

$$\begin{aligned}R_{\text{train}} &= \frac{1}{N} \|\mathbf{y} - \mathbf{A} \mathbf{X} \mathbf{w}^*\|_2^2 \\ &= \frac{r^2}{N} \text{Tr}(\mathbf{y} \mathbf{y}^\top \mathbf{Q}^2) \\ &= -\frac{r^2}{N} \frac{\partial}{\partial r} \text{Tr}(\mathbf{y} \mathbf{y}^\top \mathbf{Q}),\end{aligned}$$

as well as the empirical loss

$$(54) \quad L(\mathbf{w}^*) = r \mathbf{y}^\top \mathbf{Q} \mathbf{y} / N,$$

where we set  $\mathbf{Q} \stackrel{\text{def}}{=} (r \mathbf{I}_N + \Phi \Phi^\top)^{-1}$ .

We first define four thin matrices,

$$(55) \quad \begin{aligned} \mathbf{U} &= \begin{bmatrix} \frac{1}{\sqrt{N}} \Xi^{\text{gn}} \mathbf{y} + \frac{\lambda}{\sqrt{N}} \mathbf{y} & \frac{\lambda}{\sqrt{N}} \mathbf{y} \end{bmatrix} \in \mathbb{R}^{N \times 2} \\ \mathbf{V} &= \begin{bmatrix} \frac{\mu}{\sqrt{N}} \mathbf{u} & \frac{1}{\sqrt{N}} (\Xi^x)^\top \mathbf{y} \end{bmatrix} \in \mathbb{R}^{F \times 2}, \\ \mathbf{L} &= \begin{bmatrix} \mathbf{O} \mathbf{V} + \mathbf{U} \mathbf{V}^\top \mathbf{V} & \mathbf{U} \end{bmatrix} \in \mathbb{R}^{N \times 4}, \\ \mathbf{M} &= \begin{bmatrix} \mathbf{U} & \mathbf{O} \mathbf{V} \end{bmatrix} \in \mathbb{R}^{F \times 4}. \end{aligned}$$

where  $\mathbf{O} = \Xi^{\text{gn}} \Xi^x$ . Then

$$(56) \quad \begin{aligned} \Phi &= \mathbf{U} \mathbf{V}^\top + \mathbf{O} \\ \Phi \Phi^\top &= \mathbf{L} \mathbf{M}^\top + \mathbf{O} \mathbf{O}^\top \end{aligned}$$

Using Woodbury matrix identity, and denoting  $\mathbf{R} = (r \mathbf{I}_N + \mathbf{O} \mathbf{O}^\top)^{-1}$ , we have

$$\begin{aligned} \mathbf{Q} &= (r \mathbf{I}_N + \mathbf{O} \mathbf{O}^\top + \mathbf{L} \mathbf{M}^\top)^{-1} \\ &= (r \mathbf{I}_N + \mathbf{O} \mathbf{O}^\top)^{-1} - (r \mathbf{I}_N + \mathbf{O} \mathbf{O}^\top)^{-1} \mathbf{L} \left( \mathbf{I}_4 + \mathbf{M}^\top (r \mathbf{I}_N + \mathbf{O} \mathbf{O}^\top)^{-1} \mathbf{L} \right)^{-1} \mathbf{M}^\top (r \mathbf{I}_N + \mathbf{O} \mathbf{O}^\top)^{-1} \\ &= \mathbf{R} - \mathbf{R} \mathbf{L} (\mathbf{I}_N + \mathbf{M}^\top \mathbf{R} \mathbf{L})^{-1} \mathbf{M}^\top \mathbf{R}. \end{aligned}$$

Now (54) can be computed as

$$(57) \quad \frac{1}{N} \mathbf{y}^\top \mathbf{Q} \mathbf{y} = \underbrace{\frac{1}{N} \mathbf{y}^\top \mathbf{R} \mathbf{y}}_{\mathbb{R}^{1 \times 1}} - \underbrace{\frac{1}{\sqrt{N}} \mathbf{y}^\top \mathbf{R} \mathbf{L}}_{\mathbb{R}^{1 \times 4}} \underbrace{(\mathbf{I}_4 + \mathbf{M}^\top \mathbf{R} \mathbf{L})^{-1}}_{\mathbb{R}^{4 \times 4}} \underbrace{\frac{1}{\sqrt{N}} \mathbf{M}^\top \mathbf{R} \mathbf{y}}_{\mathbb{R}^{4 \times 1}}.$$



The curly braces indicate 25 random variables which all concentrate around their means (they are self-averaging in statistical physics terminology). Their expectations can be computed as follows:

- $\frac{1}{N} \mathbf{y}^\top \mathbf{R} \mathbf{y}$ : The first term of the RHS of 57 is a special case discussed in Section 3.2.1 [41] and also has been discussed in [12]. As Theorem 1 in [41] suggests, the Green function 51 can be computed as

$$G_{\mathbf{O}\mathbf{O}^\top}(z) = \frac{1}{z} P\left(\frac{1}{z}\right)$$

where  $P(t)$  is the solution of

$$(58) \quad P = 1 + \frac{(1 + (P-1)/\alpha)(1 + (P-1))t}{1 - (1 + (P-1)/\alpha)(1 + (P-1))Pt}.$$

Since  $\mathbf{R}$  is rotationally invariant, we have

$$\mathbb{E} \frac{1}{N} \mathbf{y}^\top \mathbf{R} \mathbf{y} = \mathbb{E} \frac{1}{N} \text{Tr}(\mathbf{y} \mathbf{y}^\top \mathbf{R}) = \mathbb{E} \frac{1}{N} \text{Tr}(\mathbf{R}) = q,$$

where  $q$  is the real solution of

$$qr = 1 - \frac{(1 + (qr-1)/\alpha)q}{1 + (1 + (qr-1)/\alpha)q}.$$

It is easy to check that when  $r \rightarrow 0$ , we have  $q \rightarrow \frac{1-\alpha}{r}$  for  $\alpha \leq 1$ .

- $\frac{1}{\sqrt{N}} \mathbf{y}^\top \mathbf{R} \mathbf{L}$  and  $\frac{1}{\sqrt{N}} \mathbf{M}^\top \mathbf{R} \mathbf{y}$ : we use (55) and recall that  $\mathbf{R} = (r\mathbf{I}_N + \mathbf{O}\mathbf{O}^\top)^{-1}$ . We get

$$\mathbb{E} \frac{1}{\sqrt{N}} \mathbf{y}^\top \mathbf{R} \mathbf{L} = \begin{bmatrix} \alpha\mu^2\lambda & \lambda & \lambda & \lambda \end{bmatrix} \times q,$$

as well as

$$\mathbb{E} \frac{1}{\sqrt{N}} \mathbf{M}^\top \mathbf{R} \mathbf{v} = \frac{1}{\sqrt{N}} \begin{bmatrix} \mathbf{U}^\top \\ \mathbb{E} \mathbf{V}^\top \mathbf{O}^\top \end{bmatrix} \mathbf{R} \mathbf{v} = \begin{bmatrix} \lambda \\ \lambda \\ 0 \\ 0 \end{bmatrix} q.$$

- $(\mathbf{I}_4 + \mathbf{M}^\top \mathbf{R} \mathbf{L})^{-1}$ : we again use (55) to first average  $\mathbf{M}^\top \mathbf{R} \mathbf{L}$ ,

$$\mathbb{E} \mathbf{M}^\top \mathbf{R} \mathbf{L} = \begin{bmatrix} \alpha\mu^2 a + \alpha\lambda^2\mu^2 q & b + \lambda^2 q & a + \lambda^2 q & \lambda^2 q \\ \alpha\lambda^2\mu^2 q & \lambda^2 q & \lambda^2 q & \lambda^2 q \\ \mu^2 c & 0 & 0 & 0 \\ \alpha\mu^2 b & d & b & 0 \end{bmatrix}.$$

We then find the (self-averaging) values that its entries are composed of,

$$(59) \quad \begin{aligned} a(\alpha, r) &= \mathbb{E} \frac{1}{N} \mathbf{y}^\top (\mathbf{\Xi}^{\text{gn}})^\top \mathbf{R} \mathbf{\Xi}^{\text{gn}} \mathbf{y} \\ b(\alpha, r) &= \mathbb{E} \frac{1}{N} \mathbf{y}^\top \mathbf{\Xi}^x \mathbf{O}^\top \mathbf{R} \mathbf{\Xi}^{\text{gn}} \mathbf{y} \\ c(\alpha, r) &= \mathbb{E} \frac{1}{N} \mathbf{u}^\top \mathbf{O}^\top \mathbf{R} \mathbf{O} \mathbf{u} \\ d(\alpha, r) &= \mathbb{E} \frac{1}{N} \mathbf{y}^\top \mathbf{R} \mathbf{\Xi}^x \mathbf{O}^\top \mathbf{R} \mathbf{O} \mathbf{\Xi}^{x^\top} \mathbf{y} \\ q(\alpha, r) &= \mathbb{E} \frac{1}{N} \mathbf{y}^\top \mathbf{R} \mathbf{y}. \end{aligned}$$

Now we have all the ingredients in the RHS of (57)/(54). Putting them together gives

$$(60) \quad \begin{aligned} L(\mathbf{w}^*) &= \frac{r}{N} \left( \mathbf{y}^\top \mathbf{R} \mathbf{L} - \mathbf{y}^\top \mathbf{R} \mathbf{L} (\mathbf{I}_4 + \mathbf{M}^\top \mathbf{R} \mathbf{L})^{-1} \mathbf{M}^\top \mathbf{R} \mathbf{y} \right) \\ &\xrightarrow{N \rightarrow \infty} r \left( q - q^2 \left( \frac{\lambda^2 (a\alpha\mu^2 + c\mu^2 - (a + (b-1)^2)) + d(a\mu^2(c-\alpha) - 1) + \alpha\mu^2 + \alpha b^2\mu^2 - 2\alpha b\mu^2 + 1}{\lambda^2 q(a\alpha\mu^2 + c\mu^2 - (a + (b-1)^2)) + d(a\mu^2(c-\alpha) - 1) + \alpha\mu^2 + \alpha b^2\mu^2 - 2\alpha b\mu^2 + 1 + \alpha\mu^2(\alpha - c) + 1} \right) \right). \end{aligned}$$

The full expressions for quantities in (59) are complicated. We thus analytically study the ridgeless limit  $r \rightarrow 0$  in which the following hold:

$$\begin{aligned} a &\rightarrow \frac{(1-\alpha)^2}{r}, \\ b &\rightarrow \alpha - \frac{\alpha^2}{(1-\alpha)^2}r, \\ c &\rightarrow \alpha - \frac{\alpha^2}{(1-\alpha)^2}r, \\ d &\rightarrow 1 - \frac{\alpha}{1-\alpha}r, \\ q &\rightarrow \frac{1-\alpha}{r} + \frac{\alpha^2}{(1-\alpha)^2}. \end{aligned}$$

Substituting into (60) yields

$$L(\mathbf{w}^*) \rightarrow \frac{(1-\alpha)(\alpha^2\mu^2+1)}{\alpha^2(\lambda^2+1)\mu^2+\alpha\lambda^2+1}.$$

Finally, undoing the rescaling  $\alpha \rightarrow \frac{1}{\gamma}$ ,  $\mu^2 \rightarrow \mu\gamma$ , we get the same expressions for  $R_{\text{train}}$  as in (15) for  $\tau = 1$ .

#### APPENDIX D. A SIGNAL PROCESSING INTERPRETATION OF SELF-LOOPS

Digital Signal Processing (DSP) provides a self-consistent, powerful and efficient framework and methodology to analyze signals on graphs [43, 47], which are usually called Graph Signal Processing (GSP) in recent literature [11, 37]. We now show a simple interpretation of negative self-loops based on that.

In homophilic graphs the labels change slowly on the graph: they are a low-pass signal [7, 37] with most of their energy concentrated on the eigenvectors of the graph Laplacian which correspond to small eigenvalues or small “frequencies”. Equivalently, they correspond to large eigenvalues of the adjacency matrix since  $\mathbf{L} = \text{diag}(\mathbf{A}\mathbf{1}) - \mathbf{A}$ .<sup>5</sup> On heterophilic graphs the labels usually change across an edge, which corresponds to a high-frequency signal concentrated on the small-eigenvalue eigenvectors of the adjacency matrix. A graph Fourier transform can be defined via the Laplacian but also via the adjacency matrix [37]. The matrix product  $\mathbf{A}\mathbf{x} = \mathbf{h}$  is a delay-like filter, diagonal in the graph Fourier domain with basis functions which are the eigenvectors  $\mathbf{u}_1, \dots, \mathbf{u}_N$  of  $\mathbf{A}$ . We have  $(\mathbf{A}\mathbf{x})_i = \langle \mathbf{x}, \mathbf{u}_i \rangle = \lambda_i \hat{\mathbf{x}}_i = \lambda_i \langle \mathbf{x}, \mathbf{u}_i \rangle$ , where  $\lambda_i$  is the  $i$ -th smallest eigenvalue of  $\mathbf{A}$ .

Figure 9 illustrates the spectra of homophilic and heterophilic labels and graphs. A homophilic graph<sup>6</sup> has a low-pass spectrum while a heterophilic graph has a high-pass spectrum. A self-loop shifts the spectrum of  $\mathbf{A}$  so that it becomes either a lowpass filter for positive  $c$  or a highpass filter for negative  $c$ . As a result, the corresponding GCNs better suppress noise and enhance signal for the corresponding graph types. In particular, assuming that the label-related signal in  $\mathbf{x}$  lives between eigenvalues  $\lambda_a$  and  $\lambda_b$  (say, negative, so we are in a heterophilic situation), we can quantify the distortion induced by the filter  $\mathbf{A} + c\mathbf{I}$  as  $(\lambda_a + c)/(\lambda_b + c)$  which is close to 1 for large  $|c|$ .

#### APPENDIX E. DOUBLE DESCENT IN VARIOUS GNNs

In Figure 10 we experiment with node classification on the **Citeseer** dataset and some popular GNN architectures: the graph attention network [50], GraphSAGE [19], and chebyshev graph network [8]. The architectures of these GNNs incorporate various strategies to mitigate overfitting. As a result there is no clear double descent in the test accuracy curves, but we still observe non-monotonicity in the test risk.

<sup>5</sup>If node degrees are all the same the eigenvectors of the adjacency matrix and the Laplacian coincide.

<sup>6</sup>More precisely, a homophilic graph-label pair.

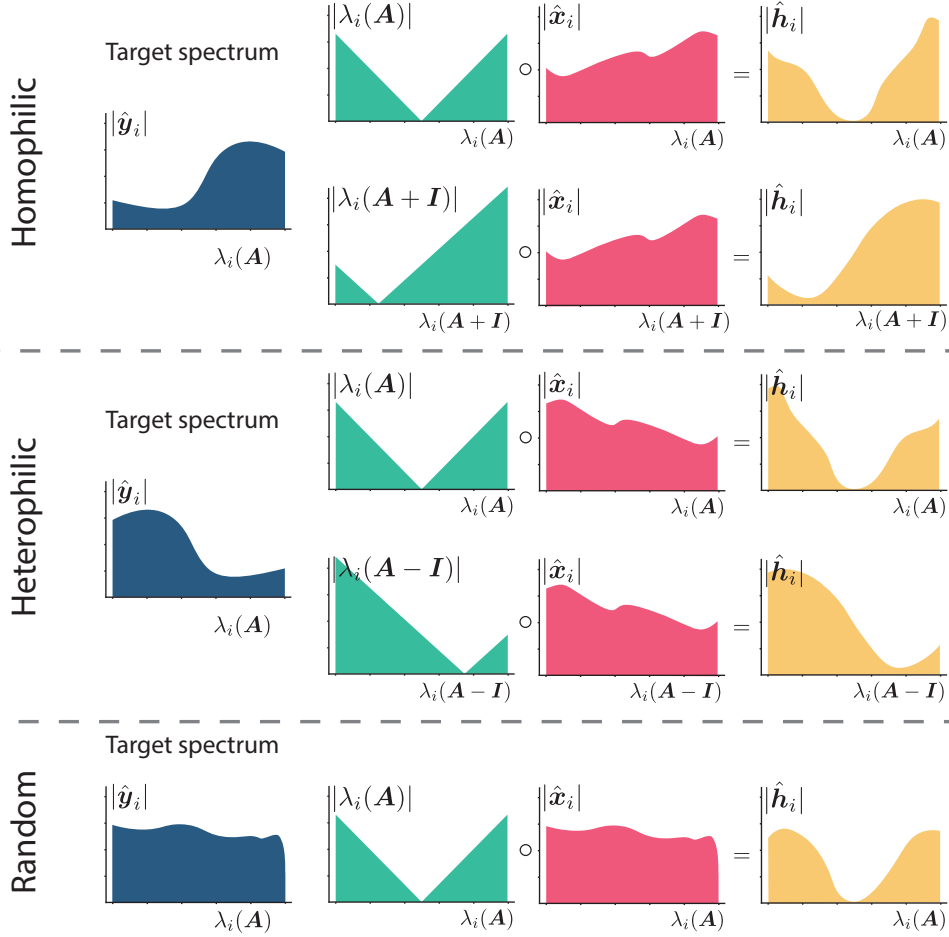


FIGURE 9. Spectral understanding of self-loops in GCNs. The first (blue) column shows the spectrum of the true signal for different types of graphs. The following three columns illustrate  $\mathbf{A}\mathbf{x} = \mathbf{h}$  in the graph spectrum domain ordered as in the adjacency matrix so that the high frequencies are on the left. The signal  $\mathbf{x}$  is the noisy signal,  $\mathbf{x} = \mathbf{y} + \boldsymbol{\xi}$ . In the homophilic case, compared with  $\mathbf{A}\mathbf{x}$ , the spectrum of  $(\mathbf{A} + \mathbf{I})\mathbf{x}$  is closer to the spectrum of the true signal  $\mathbf{y}$ ; in the heterophilic case, compared with  $\mathbf{A}\mathbf{x}$ , the spectrum of  $(\mathbf{A} - \mathbf{I})\mathbf{x}$  is closer to the spectrum of the true signal  $\mathbf{y}$ .

#### APPENDIX F. EXPERIMENTAL DETAILS

All GNNs in Figure 3 are trained by the ADAM optimizer with learning rate  $10^{-2}$  and weight decay  $10^{-5}$ . We run ADAM for  $10^4$  iterations and use the weights from the iteration with minimal training loss as the final weights. In each trial, the training and test nodes are selected randomly. We sample training nodes separately for each label to avoid the pathology where a label has few or zero samples, which can happen at extremely low training ratios. We average 10 different trials for each point; the error bars show their standard deviation. The standard deviation in the plots mainly comes from the train-test splits in the different trials; The variation due to random initialization and stochastic optimization is comparatively small.

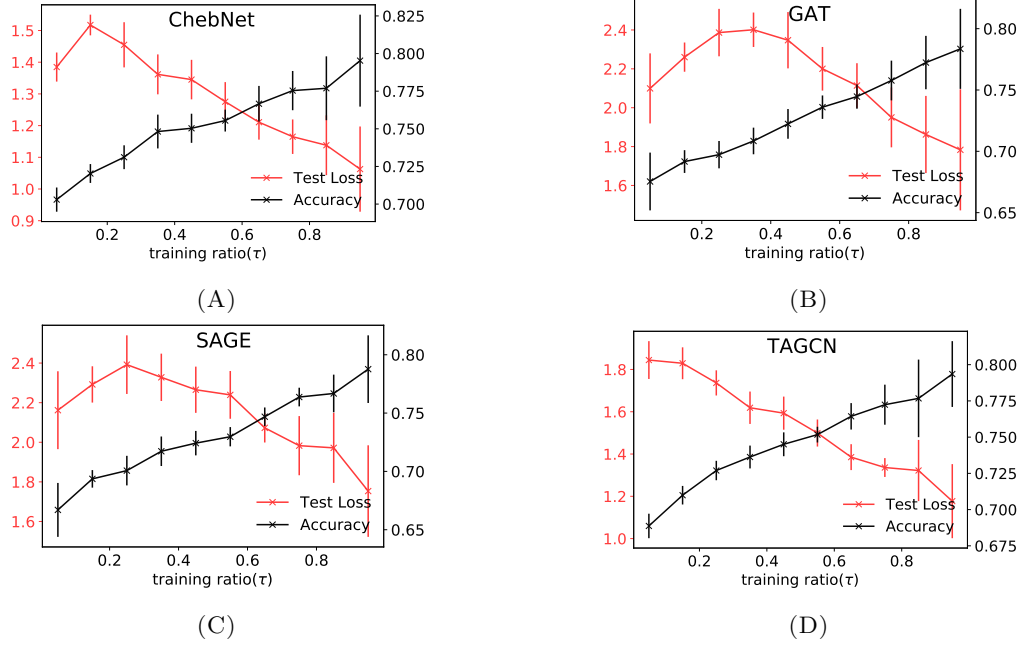


FIGURE 10. Test risk and classification accuracy at different training ratios for Chebyshev GNN (ChebNet), graph attention network (GAT), the graph sample and aggregate network (SAGE), topology adaptive graph convolutional networks (TAGCN), on the Citeseer dataset. All models have two layers with ReLU activations, and are trained by ADAM with the cross-entropy loss.